Electrode Materials

International Edition: DOI: 10.1002/anie.201409262
German Edition: DOI: 10.1002/ange.201409262

Nickel-Rich Layered Lithium Transition-Metal Oxide for High-Energy Lithium-Ion Batteries

*Wen Liu, Pilgun Oh, Xien Liu, Min-Joon Lee, Woongrae Cho, Sujong Chae, Youngsik Kim, and Jaephil Cho**

Keywords:
cation mixing · layered structure · lithium-ion batteries · nickel · surface reactions

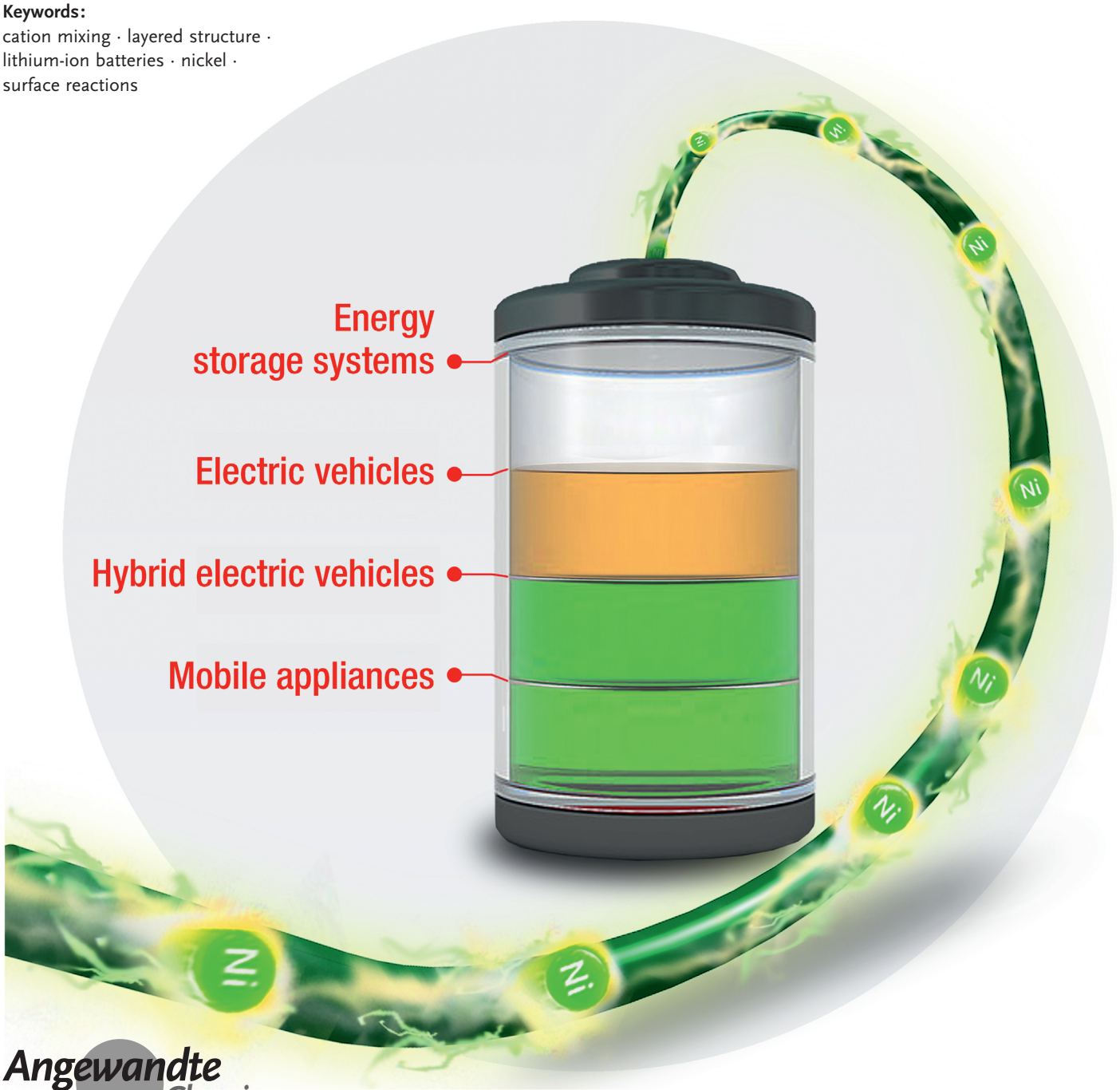

High energy-density lithium-ion batteries are in demand for portable electronic devices and electrical vehicles. Since the energy density of the batteries relies heavily on the cathode material used, major research efforts have been made to develop alternative cathode materials with a higher degree of lithium utilization and specific energy density. In particular, layered, Ni-rich, lithium transition-metal oxides can deliver higher capacity at lower cost than the conventional $LiCoO_2$. However, for these Ni-rich compounds there are still several problems associated with their cycle life, thermal stability, and safety. Herein the performance enhancement of Ni-rich cathode materials through structure tuning or interface engineering is summarized. The underlying mechanisms and remaining challenges will also be discussed.

From the Contents

1. Introduction 4441
2. Structure and Reaction Mechanism 4443
3. Issues and Challenges of Ni-based Cathode Materials 4444
4. Recent Progress 4447
5. Remaining Challenges 4452
6. Summary and Outlook 4455

1. Introduction

In face of growing pressure on resources and the environmental crisis, developing renewable energy and energy conservation are considered to be essential technical issues.[1] Therefore, energy-storage technology is more critical today than ever before. As the new type of removable energy-storage device, lithium-ion batteries (LIBs) are expected to be widely used in devise applications, such as stationary energy storage, smart grid, electric transportation.[1a,2] Further increasing the energy density and reducing the cost are main directions of developments in LIBs. The performance of LIBs, such as output potential, energy density, power density, lifetime, and safety, are strongly depending on the properties of the materials deployed.[3] To date, the increases in energy storage in LIBs is mainly attributed to cell design rather than material evolution, and in terms of material evolution much more progress seems to have been made with the anode materials than with the cathode materials.[4] Conventional layered structural $LiCoO_2$ (LCO) has been widely used in small LIBs for consumer electronics, such as mobile phones, cameras, laptops, MP3 players. However, the LCO cathode can only store a relatively small amount of charge, up to 160 mAh g^{-1}, with lithium utilization in the structure less than 60 %. Clearly, the energy density of the cathode material has been a bottle neck, especially concerning LIBs for transportation and stationary energy storage.

Over the past two decades, these requirements of higher utilization of lithium and specific energy density have been the main driving force for the advance of alternative layered-structure compounds, such as olivine phosphates ($LiMPO_4$; M = Fe, Co, Ni, and Mn) and spinel oxides (LiM_2O_4, M = Mn, Ni and Co), however these have a low capacity.[4a,5] Schematic illustrations of the three main kinds of cathode materials and their corresponding electrochemical properties are shown in Figure 1. The layered structural compounds can be represented by the formula $LiMO_2$ (M = transitional-metal elements), where the M and Li ions are located in octahedral sites in a face-centered cubic oxygen structure. Li slabs lie between MO_2 slabs in the [111] direction of the cubic structure. M are typically electrochemically active transitional-metal ions, such as manganese, nickel, or cobalt. It is widely established that the diffusion of Li^+ ions in the layered structures occurs along a two-dimensional (2D) interstitial space, which is considered as a pathway for higher Li^+ mobility. The $LiMO_2$ cathode can produce a very large theoretical capacity of more than 270 mAh g^{-1} and a comparatively high working voltage above 3.6 V versus Li metal.[6] Therefore, the layered-structure $LiMO_2$ is meant to facilitate the design of lithium-ion batteries with high energy density. However, it is believed that $Li_{1-x}CoO_2$ becomes unstable in a highly delithiated state with high voltages above 4.3 V, leading to accelerated capacity fading and exothermic reactions with organic electrolytes. Replacing Co with Ni in the layered structure results in higher utilization of lithium, approaching a capacity of 220 mA h g^{-1} with almost 80 % reversible extraction of Li in the host structure. A number of Ni-based derivatives have been studied and characterized. These cathode materials are capable of reaching capacities of over 220 mA h g^{-1}, and are fairly compatible with the electrolytes. The energy density of Ni-rich cathode materials can approach 800 Wh kg^{-1} (Figure 1 d). However, owing to the similar radius of Li^+ (0.076 nm) and Ni^{2+} (0.069 nm), non-stoichiometric structures are usually found as the result of Li/Ni site-exchange. This phenomenon is termed cation mixing and causes various problems including capacity loss and structure deterioration,[7] surface side reactions that accelerate capacity fade

[*] Dr. W. Liu,[+] P. Oh,[+] Dr. X. Liu, M.-J. Lee, W. Cho, S. Chae, Prof. Dr. Y. Kim, Prof. Dr. J. Cho
Department of Energy Engineering and School of Energy and Chemical Engineering, Ulsan National Institute of Science and Technology (UNIST)
Ulsan, 689-798 (Republic of Korea)
E-mail: jpcho@unist.ac.kr
Homepage: http://www.jpcho.com
[+] These authors contributed equally to this work.

Supporting information for this article is available on the WWW under http://dx.doi.org/10.1002/anie.201409262.

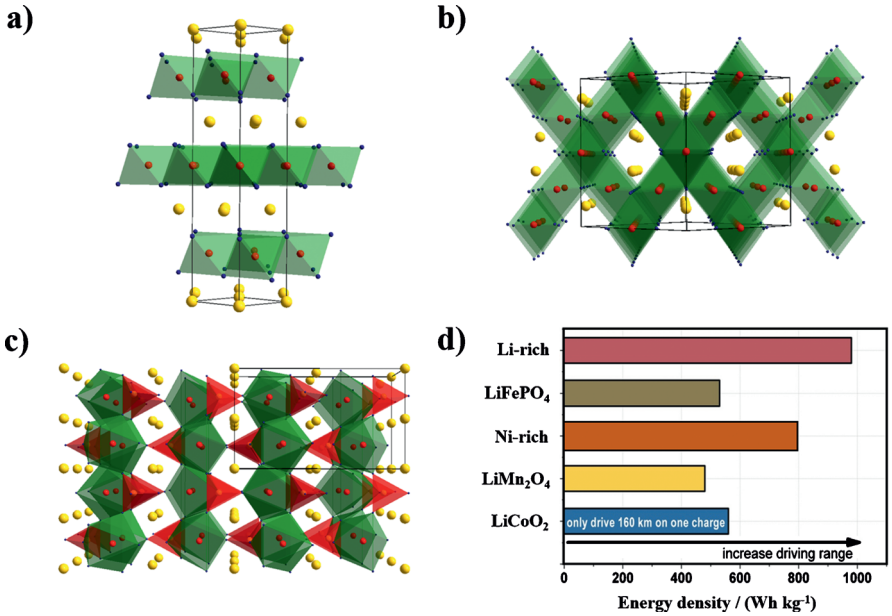

Figure 1. Illustration of the crystal structures of the main cathode materials: a) $LiCoO_2$ with layered structure, b) $LiMn_2O_4$ with spinel structure, c) $LiFePO_4$ with olivine structure. d) Energy density of typical cathode materials.[83] Copyright: Wiley-VCH, 2014.

during cycling and high-temperature storage,[8] poor thermal stability, and dramatic heat release from the electrode if it becomes highly delithiated.[9] To overcome the performance degradation and improve battery safety, several strategies have been proposed and demonstrated (Figure 2). In terms of good reversibility, the structural stability of cathode materials needs to be maintained during the repeated Li^+ insertion/extraction. However, cation mixing causes not only the non-stoichiometric structure of Ni-rich materials, but also the structure degradation and capacity fading upon cycling at 60 °C. This degradation usually is associated with a structural transformation to spinel-like and NiO-type rock-salt phases. To improve the performance degradation and enhance safety, cation substitution and structural doping have been proposed and demonstrated. The charge transportation, structure deterioration, and their effects on stability can be observed through a combination of structure analysis and electrochemical methods. Electrolyte decomposition on the surface of the electrode materials results in the formation of a solid-state electrolyte interface (SEI). The SEI layer is involved in the charge-transfer reaction between the bulk and electrolyte, although the solid-state diffusion of Li^+ has been considered as the rate-determining step of the electrochemical reaction. Thus, formation of a stable and highly ionic conductive interphase is critical for cycleability and rate capacity. The surface-coating strategy improves both the cycle performance and safety properties of batteries. However, the microstructure and composition of the surface layers should be further understood by in situ/ex situ spectroscopic studies.

Herein, we review the recent development of Ni-based layered lithium transition-metal oxides as cathodes for high energy-density LIBs (Figure 3). Furthermore, we wish to show that the most crucial drawbacks of the materials are structural instability and their surface chemistry. Through examples we elucidate the structure–performance relationships, and the effects of material modifications. From the insight thus gained, we propose new research directions and give an outlook for fundamental improvements in Ni-rich materials. In this respect, this Review differs from other Review articles

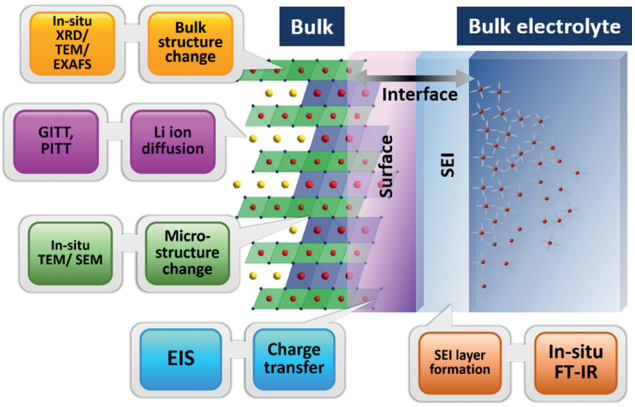

Figure 2. Schematic diagram of the degradation mechanisms of Ni-rich cathode materials, and the strategies and investigation techniques to study them.

Jaephil Cho is a Professor and the head of the School of Energy and Chemical Engineering at UNIST (Korea). He is a director of the Green Energy Materials Developed Center (funded by the Ministry of Science, ICT&Future Planning) and Samsung SDI-UNIST Future Battery Research Center. His current research is focused mainly on Li-ion and metal–air batteries, and redox-flow batteries for energy storage.

Wen Liu is a postdoctoral researcher with Prof. Jaephil Cho at the School of Energy and Chemical Engineering at UNIST (Korea). He received his Ph.D. (2013) in Chemistry with Prof. Henghui Zhou from Peking University (China). His research interests include the synthesis of functional materials and their applications in lithium-ion batteries and electrochemical catalysts.

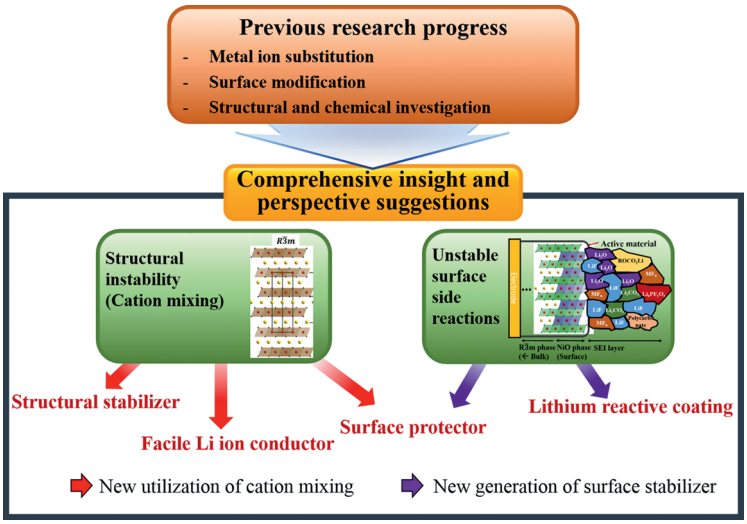

Figure 3. New insights into Ni-rich based cathode materials.

which present previous research progress and its limits.[5c,10] Especially, the new insights into "cation mixing" and suggestions for the surface-modification method in this Review lead to a new concept for materials design and the utilization of not only Ni-rich materials, but also generally for layered cathodes for LIBs including $LiCoO_2$ and Li-rich materials.

2. Structure and Reaction Mechanism

It is believed that the high reversible capacity of Ni-rich materials is due to their electronic structure. From the electronic structure point of view shown in Figure 4a, the position of $Ni^{3+/4+}$ in the e_g energy band overlaps with the top of the O^{2-} 2p band less than the $Co^{3+/4+}$ t_{2g} band does indicating there is less electron delocalization with $Ni^{3+/4+}$.[11] Because of the overlap of the $Co^{3+/4+}$ t_{2g} band with the top of O^{2-} 2p band, the Co^{4+} state, which can only be attained if more than 0.5 Li is extracted from $LiCoO_2$, cannot be accessed without encountering chemical instability and safety concerns. In contrast, the Ni^{4+} state can be achieved in a layered material with much higher utilization of lithium in the host structure, approaching capacity of 220 mAh g^{-1}. However, as a practical electrode material, several major drawbacks brought out by the intrinsic properties have to be circumvented before application. The first issue is that of non-stoichiometric structure. The non-stoichiometric structure leads to partial reduction of Ni ion's valence from +3 to +2, and the partial reduction causes local structure collapse of the interlayer space, and transition-metal ions migrate from the transition-metal layer to the lithium layer.[12] (This cation migration from TM layer to Li layer is called "cation mixing".) The charge–discharge process of $LiNiO_2$ involves several phase transitions, which in repeated cycling decrease the stability of electrode. Ohzuku et al.[13] and Delmas et al.[14] divided the material into four reaction regions of $Li_{1-x}NiO_2$ in terms of the variation in lattice parameters (Figure 5a). In this regard, different models of phase transition and $LiNiO_2$–NiO_2 pseudo-binary phase diagrams have also been proposed through means of in situ X-ray diffraction (XRD) experiments and ab initio calculations,[15] as depicted in Figure 5b. At high potential and elevated temperature, nickel dissolution from the surface of $LiNiO_2$ accelerates the structural instability. This side reaction is normally accompanied by a partial structure transformation to spinel and NiO-type rock-salt phases. The delithiated electrode is thermodynamically metastable and exhibits low thermal stability, raising serious safety concerns. To inhibit the cation disorder and improve the structural stability, partial substitution of Ni^{2+} with other metal ions in the transition-metal layers has been undertaken, forming layered Li-Ni-Co-Mn-O compounds (Figure 4b).

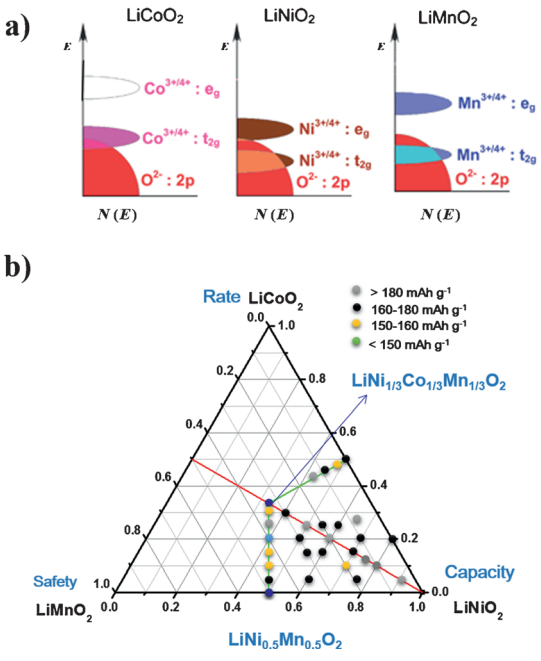

Figure 4. a) Schematic illustration of the electronic structure of $LiCoO_2$, $LiNiO_2$, and $LiMnO_2$.[11] b) Compositional phase diagrams of lithium stoichiometric-layered transition-metal oxide: $LiCoO_2$-$LiNiO_2$-$LiMnO_2$. The positions indicated by dots represent the described $LiNi_{1-x-y}Co_xMn_yO_2$ materials Copyright: Royal Society of Chemistry, 2008.

Pilgun Oh is a Ph.D. student with Prof. Jaephil Choat the School of Energy and Chemical Engineering at UNIST (Korea) since 2011. His current research is focused on structural characterization and material modification methods of cathode materials for lithium ion batteries.

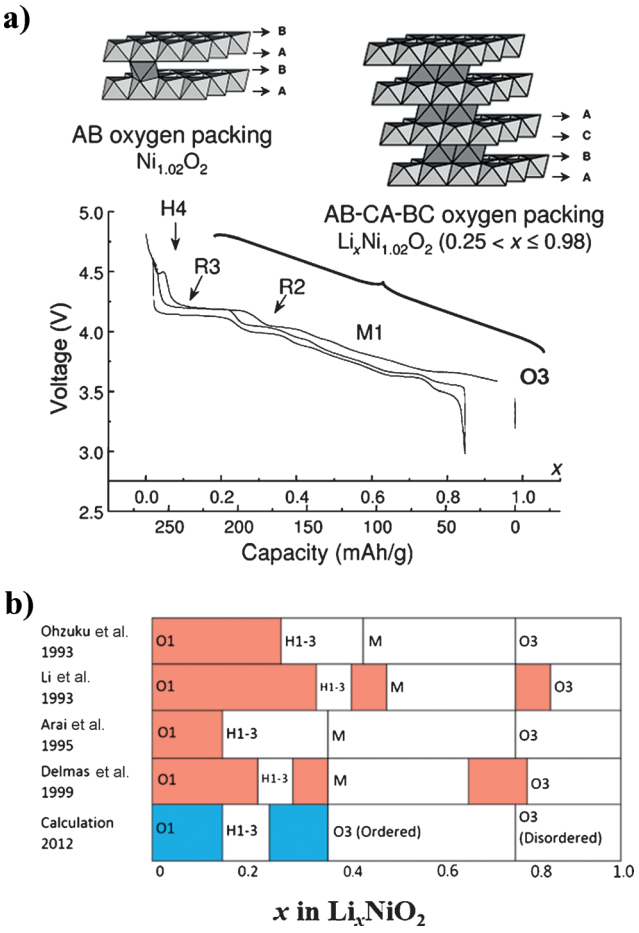

Figure 5. Structural changes of $Li_{1-x}NiO_2$ during the electrochemical process. a) Cycling curve obtained for a $Li//Li_xNi_{1.02}O_2$ cell cycled at low rate (C/100).[14] O3, M1, H2, H3 are characterized by AB-CA-BC oxygen packing, whereas O1 is characterized by AB oxygen packing. Copyright: Cambridge University Press, 2002. b) Phase diagram of the $LiNiO_2$-NiO_2 pseudo-binary system from experimental data and calculation.[14d,15d] Copyright: Elsevier, 2012.

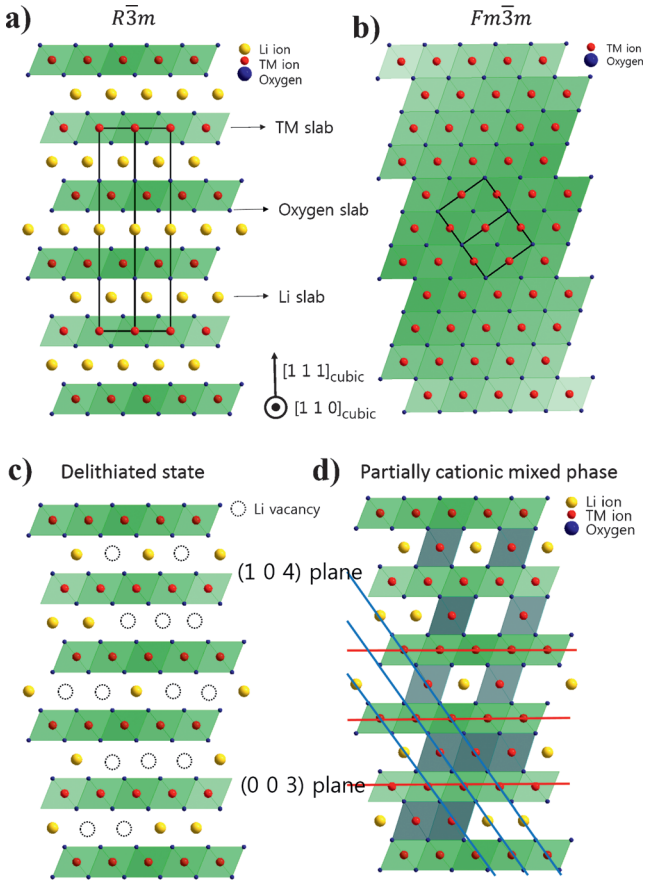

Figure 6. Illustration of the ordered and disordered phase in layered lithium metal oxides and their structural transformation. a) Well-ordered $R\bar{3}m$ structure; b) The cation disorder or cation mixing phase with $Fm\bar{3}m$ structure; c) $R\bar{3}m$ structure with Li vacancies in highly charged state; d) Partially cation mixed phase with TM ions in Li slab. Li atoms yellow, transition metals red, coordinated oxygen atoms dark blue.

3. Issues and Challenges of Ni-based Cathode Materials

3.1. Cation Mixing

As mentioned before, structural stability of Ni-rich materials is closely related to "cation mixing", which involves cations disordering between transition-metal sites (octahedral 3a site) and lithium sites (octahedral 3b site).[16] General layered materials (Figure 6a), have $R\bar{3}m$ structure which is a repeating O3 structure of oxygen-lithium-oxygen-TM-oxygen-lithium-oxygen-TM-oxygen along the rhombohedral [001] direction (=spinel [111] direction).[16e] Therefore, a perfect $R\bar{3}m$ structure has clearly separated transition-metal sites (3a) and lithium sites (3b). The Ni ion has tendency to be formed as Ni^{2+} in the FCC octahedral site rather than Ni^{3+} because Ni^{3+} is, according to crystal-field theory, unstable because of the unpaired electron spin of the e orbitals.[16d] The ionic radius of Ni^{2+} is 0.69 Å, which is similar to the ionic radius of Li^+ (0.76 Å). Owing to this similarity of ion size, Ni^{2+} ions easily occupy 3b lithium sites in the Li slab, giving rise to the "cation mixing" or "cation disorder" (Figure 6b).[17]

Compared to the well-ordered phase the disordered phase has a higher activation energy barrier for lithium diffusion owing to its smaller distance between the slabs, and also a lower lithium diffusivity because of hindrance caused by the transition metal in the lithium layer.[16f,18] Therefore, the rate capability of the active material decreases with the increasing cation mixing. Many methods have been tried to reduce this disordering by controlling the lithiation conditions.[16c,19] For example, based on first principle calculations, Ceder et al. suggested synthesis conditions for forming stable phases of Ni-rich materials depending upon the lithiation temperature.[16e] Meanwhile, many attempts to measure the degree of the disordering have been developed. The most popular method is X-ray diffraction analysis.[16i] When cation disorder is generated, transition-metal ions occupy the lithium sites as in Figure 6d. The disordering leads to a partial destructive interference of the (003) plane's constructive interference at a Bragg angle of $\theta_{d(003)}$ and a decrease in intensity of the (003) peak. In contrast, for the (104) peak, its intensity increases

because transition-metal ions in the lithium layer are also on the (104) plane, leading to increased constructive interference of the peaks for (104) planes. As a result, intensity ratio of the (003)/(104) peaks decreases as the degree of the disordering increases. Earlier researchers tried to synthesize less-disordered Ni-rich materials for which the (003)/(104) intensity ratio is higher than 1.2.[19c]

This cation migration from the transition-metal site to Li site occurs not only during the material synthesis procedure but also the electrochemical cycling process.[16a,18,20] For example, Shao-horn et al. reported cation migration from the transition-metal slab to Li slab during electrochemical cycles by using TEM analysis.[16d] In addition, Kang et al. reported that $LiNi_{0.5}Co_{0.2}Mn_{0.3}O_2$ undergoes the phase transition from $R\bar{3}m$ to spinel-like and $F\bar{3}m$ during electrochemical cycles just like Li-rich materials.[20a] In a highly charged state (4.8 V charged state), the material has an extremely unstable structure because of the empty lithium sites, and this instability leads to transition-metal-ion migration from the transition-metal layer to the lithium layer. The transition-metal ion migration has a tendency to occupy every second Li vacancy because the disordered cations repel each other (Figure 6c,d).

Accordingly, the structure in the Figure 6d shows a spinel-like phase, which however is far from being a well-ordered spinel phase.[21] Therefore, there are no reports of the formation of well-ordered spinel structure in layered materials (including Ni-rich and Li-rich materials) during electrochemical cycles. Rather, most of the previous results, which reported a phase transition of layered materials during electrochemical cycles, showed the formation of cation mixed phases or uncertain spinel phases after the cycles.[16a,18] It would be interesting to know whether or not the cation mixing layer consisted of only Ni^{2+} and oxygen ions. Recently, Doeff et al. reported the surface-deterioration mechanism of $LiNi_{0.4}Mn_{0.4}Co_{0.18}Ti_{0.02}O_2$ during the cycling process and the formation of a cation mixed phase after electrochemical cycling.[16a] Additionally, by using electron energy loss spectroscopy (EELS) analysis, they found the existence of Mn^{2+} and Co^{2+} ions in the cation mixed phase at the surface of the active material after cycling. This result supports the cation mixing layer consisting of not only Ni^{2+} ions but also of other metal ions, such as Mn^{2+} and Co^{2+} ions.

This kind of the cation disordering is currently been reconsidered as a way to stabilize the surface of active materials. Recently, Cho et al. reported a Ni-based heterostructure material which has a thin cation disordered layer induced by its high manganese concentration on the $LiNi_{0.7}Co_{0.15}Mn_{0.15}O_2$ material's surface (Figure 7).[22] This heterostructure showed improved cycling during an elevated-temperature test (60 °C). Note that the very low Li ion content in the cation mixed phase leads to a higher chemical stability than found for other delithiated cathode materials in a high state of charge (SOC) and reduces unstable side reactions between the electrolyte and the active materials. Furthermore, this phase gives a "pillar effect", which effectively prevents continuous migration of TM ions to lithium sites. This is because the Ni^{2+} ions in the Li sites provide an electrostatic repulsion force to hinder further

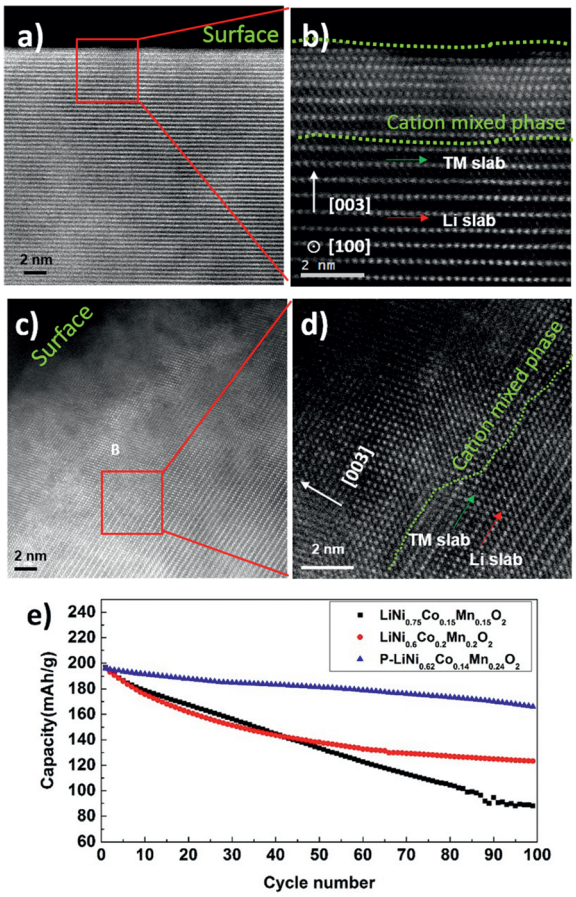

Figure 7. a,c) STEM images of a primary particle at the surface region of bare $LiNi_{0.7}Co_{0.15}Mn_{0.15}O_2$ and surface pillared $LiNi_{0.62}Co_{0.14}Mn_{0.24}O_2$.[22] b,d) High-resolution STEM images of red-marked region in (a) and (c). e) Plot of discharge capacity versus cycle number of $LiNi_{0.7}Co_{0.15}Mn_{0.15}O_2$, $LiNi_{0.6}Co_{0.2}Mn_{0.2}O_2$ as reference material, and $LiNi_{0.62}Co_{0.14}Mn_{0.24}O_2$ as surface pillared material. Copyright: American Chemical Society, 2013.

cation migration. In addition, recently Ceder et al. suggested a different theory about the facile Li-ion diffusivity in this cation disordered phase. Disordered phases in lithium-excess materials ($Li_{1+x}M_{1-x}O_2$, $x \geq 0.2$) such as Li-rich materials, can have a respectable lithium diffusivity in contrast to the cation-mixing phase in conventional layered materials ($LiMO_2$) which showed very low lithium diffusivity.[18] The facile Li-ion diffusion takes place from the O-TM channel which is surrounded by Li ions instead of TM ions.

Meanwhile, it seems that the partial cation mixing contributes to Ni-rich materials having a higher capacity than $LiCoO_2$ (LCO). In previous reports, it was supposed that the practical capacity difference between these two active materials was a result of from their respective density of states (DoS), and the tendency of $LiCoO_2$ to lose oxygen at lower SOC (ca. 0.6 Li mol) than Ni-rich materials (ca. 0.7 Li mol).[23] However, recent studies of the $LiCoO_2$ structure reported that atomic rearrangement during electrochemical de-lithiation highly depended on the structural ordering of Li ions and Li vacancies, rather than loss of oxygen.[24] For $LiCoO_2$, the cation-mixing phase between Li ions and Co ions is hardly

generated during electrochemical cycles, because the Co^{3+} or Co^{4+} ions in $LiCoO_2$ have too small an ionic radius to occupy lithium sites. Therefore, there are many unoccupied Li sites (Li vacancies) in $LiCoO_2$ in a high state of charge (SOC), over 4.5 V. The Li vacancies lead to large repulsion forces between the oxygen layers which induces structural instability. From this structural instability, structural transition occurs from O3 to P3 and O1 as the SOC increases (Figure 8a).[25] On the other hand, Ni-rich materials have much less electrostatic repulsion between the oxygen layers even in a highly delithiated state because of the cation mixing which places Ni^{2+} ions in the lithium sites (Figure 6d). Therefore, in the Ni-rich materials a rapid structural change to O1 is suppressed because the repulsion between the oxygen layers is lower (Figure 8b) and the material can realize a higher practical capacity (ca. 200 mAh g^{-1}) than $LiCoO_2$ (ca. 165 mAh g^{-1}).[15b] However, these Ni-rich materials undergo a continuous structural change from $R\bar{3}m$ to $Fm\bar{3}m$ during electrochemical cycles, which is caused by Ni^{2+} ion migration. Since this transition migration destroys active lithium sites, the structural change results in a gradual capacity decline as the number of cycles increases, when compared with $LiCoO_2$. (Details for the reason of high specific energy density of Ni-based materials are discussed in the Supporting Information.)

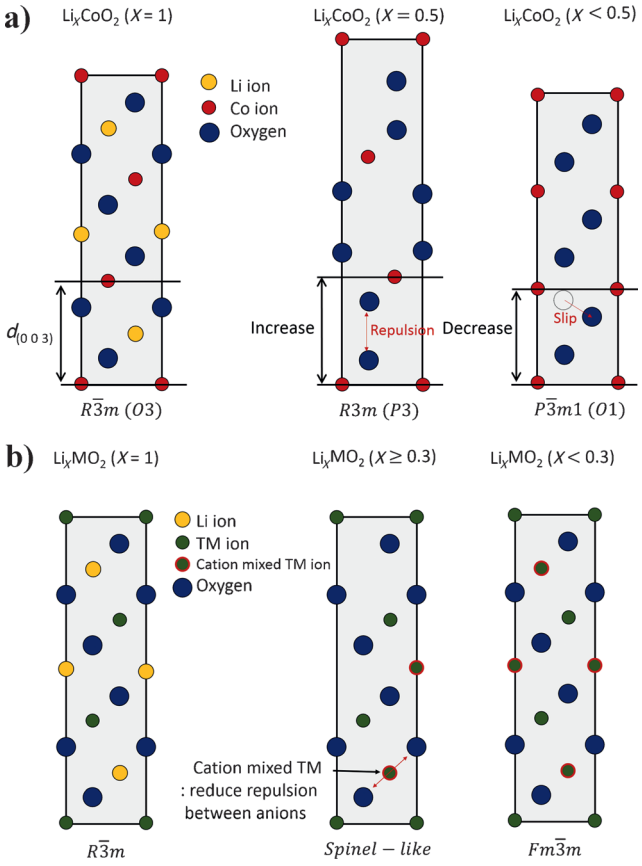

Figure 8. Crystal model of the structure evolution of $LiCoO_2$ and Ni-rich material during cation mixing. a) The structure of $LiCoO_2$ transforms from O3 to P3 and O1 as the state of charge (SOC) increases. b) Ni-rich material with cation mixing transforms from the $R\bar{3}m$ structure to the spinel-like and NiO-like rock salt $Fm\bar{3}m$ structure (see also Figure S1 in the Supporting Information).

In conclusion, the cation mixing layer, which was first considered only as the origin of performance degeneration, is currently reassessed as a surface stabilizer and facile Li-ion conductor. Therefore, an exact understanding and proper application of this phase would lead to layered cathode material's with new functions and properties.

3.2. Surface Chemistry and Side Reactions

Ni-rich layered compounds are expected to be very appealing in terms of high capacity and low cost. However, contaminating species are usually found on the surface; these result from side reactions with air and moisture during storage in an ambient environment. These surface residual species can react with electrolyte forming insulating materials on the surface of the electrode. In addition, highly reactive Ni^{4+} ions can accelerate electrolyte decomposition, leading to electrolyte depletion and a thick solid-state electrolyte interface layer. In fact, the surface chemistry and side reactions have a decisive impact on the performance of Ni-rich cathode materials for LIBs.

The presence of lithium residual species on the surface of $LiNiO_2$ and its analogues $LiNi_{1-x-y}Co_xMn_yO_2$ has been known for a long time.[26] Since the excess of lithium is necessary to produce highly ordered Ni-rich layer compounds,[27] residual lithium can remain on the surface of the active materials, and react with air. As shown in Figure 9a, the outer part of the cathode particle is contaminated with moisture and CO_2 from contact with the air, thus forming LiOH and Li_2CO_3.[28] For these reasons, the pH value of Ni-rich compounds in powder form in water is usually over 12, which results in rapid formation of a composites gel in NMP solvent.

Spontaneous side reactions also occur on the surface of Ni-rich materials through contact with electrolytes (Figure 9b). Several types of compounds are created on the surface of electrode and their composition is strongly related to the type of electrolyte used. In case of $LiClO_4$ as the lithium salt and PC (propylene carbonate) is used as the electrolyte, the major reaction is the formation of Li carbonate, whereas the formation of P/O/F containing compounds dominates when $LiPF_6$-EC (ethylene carbonate)/DMC (dimethyl carbonate) electrolyte is used.[8b] These layers, such as LiF, Li_xCO_3, and LiOH, coexist on the surface of the active materials, so that they can impede the diffusion of Li^+ ions due to their insulating properties, and thus deteriorate the electrochemical performance. Anderson et al. examined electrode samples from 18650-type lithium-ion cells which they subjected to accelerated calendar life testing.[29] The results from electrochemically treated samples showed surface-film formation on both electrodes (cathode and anode). The surface of the positive electrode laminate contained mixture of species that include polycarbonates, LiF, Li_xPF_y-type, and $Li_xPF_yO_z$-type compounds, regardless of test temperature, test duration, and state of charge.

The electrodes in LIBs are always covered by surface films, which depend on the interactions between electrodes

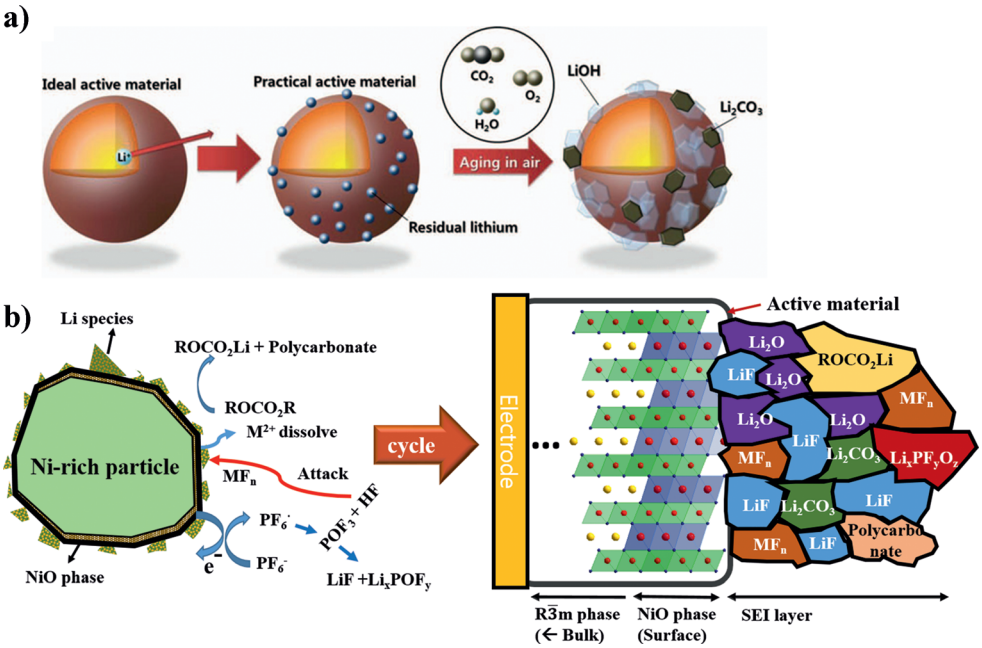

Figure 9. Illustration of the surface changes of Ni-rich cathode materials. a) Surface change of Ni-rich materials after exposure in air.[28a] Copyright: the Electrochemical Society, 2014. b) The microstructure and composition of the solid-electrolyte interface at the surface of Ni-rich cathode materials.

and solution species. These surface films strongly affect the impedance and kinetics of these electrodes. Zhuang et al. specifically emphasized the issue of capacity- and power losses of $LiNi_{0.8}Co_{0.15}Al_{0.05}O_2$ cathodes that resulted from the formation of surface species on long-term air exposure.[30] Approximately 10 nm thick surface contaminate layers can severely reduce both accessible capacity and rate capability. The cycle and rate property decline is proposed to result from particle isolation, that is, the electrical separation of active materials from the current collector. The solid-state electrolyte interface (SEI) layer, which contains various organic and inorganic electrolyte decomposition products, reduces Li^+ ion diffusivity during a charge and discharge process. Chen et al. further confirmed, by using a symmetric cell approach, that the major cause of the increase in impedance was charge-transfer resistance at the electrode/electrolyte interface.[31] Overall, residual lithium species and water on the cathode material particles are severely detrimental to cell performance in terms of both capacity retention and rate capability, especially at elevated temperature. Therefore, surface contaminations and side reactions of Ni-based cathode materials play critical roles in the power and energy stability of LIBs, and they decreasing them needs to be further addressed through surface engineering to modify the surface chemistry and properties.

4. Recent Progress

4.1. The Role of Doping Effects

Integration of extrinsic metal ions into the host structure as dopants has been extensively employed in many studies to address the structural instability of electrode materials, which is the main reason for capacity fading in Ni-rich materials.[16f,32] Although the stabilization mechanisms of each dopant element on Ni-rich materials are still uncertain, the doping effects can be divided into three forms: 1) decreasing the number of unstable elements, such as Li and Ni, by substituting them with electrochemically and structurally stable elements;[32a,b] 2) preventing Ni^{2+} ion migration from the transition-metal slab to the Li slab during electrochemical cycles by stabilizing the Ni ion's valence or forming electrostatic repulsion;[16b,33] 3) increasing the bonding strength between oxygen and metal ions, resulting in structural stability and decreased oxygen release.[16f,34] The commonly used dopant elements are Al,[32e,33,35] Mg,[36] Ti,[16a,32j,37] Cr,[38] Ga,[32i,36a,39] and Fe.[40]

After reports of partial Ni-ion substitution by Co ions, extensive studies have focused on Ni-ion substitution by Co and Mn ions for lowering cost and enhancing performance.[41] As the results of those doping researches, three kinds of solid-solution systems ($LiNiO_2$-$LiCoO_2$/$LiNiO_2$-$LiMnO_2$/$LiNiO_2$-$LiCoO_2$-$LiMnO_2$) were introduced.[42] These solid-solution systems gave superior electrochemical and thermal performance to pristine $LiNiO_2$ materials, as summarized in Figure 10.[43] Note that higher Ni content leads to higher capacity with accelerated capacity fading and poorer thermal properties.

Al is the most commonly used doping element because of its stabilizing effect on layered cathode materials.[35e] In general, a material's discharge capacity decreases with the increasing dopant concentration, whereas structural stability increases as the concentration increases.[16f,32b] Therefore, much research in Ni-rich materials has tried to optimize the doping ratio to maximize the stabilize effect with a minimum amount of dopant.[33,44] Studies for Al doping of Ni-rich materials in the past decade are mainly focused on low Al compositions below 5% concentration which hardly reduces the active material's discharge capacity.[30,44,45] However, as thermal stability and high temperature cycle ability of Ni-rich materials are considered to be more critical problems, recent research has tended to increase the Al ratio to improve the material's stability, even though it causes slight capacity loss.[46] For instance, recently our group reported $LiNi_{0.81}Co_{0.1}Al_{0.09}O_2$, which realized a higher rate and better thermal stability than $LiNi_{1-x-0.05}Co_xAl_{0.05}O_2$ along with a reversible capacity of 199 mAh g^{-1}.

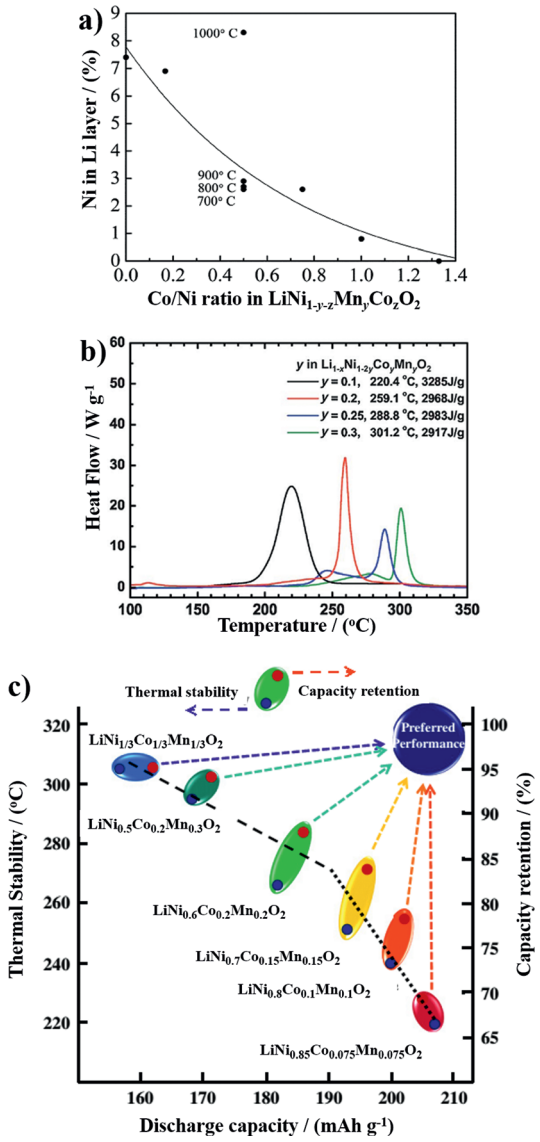

Figure 10. The composition–performance relationship of Li stoichiometric transition-metal oxides. a) The occupancy of nickel in the lithium layer versus the Co/Ni ratio in Ni-rich materials.[84] Copyright: Royal Society of Chemistry, 2004. b) The DSC data of Ni-rich materials charged to 4.3 V.[85] Copyright: the Electrochemical Society, 2007. c) A map of the relationship between discharge capacity, thermal stability, and capacity retention.[43] Copyright: Elsevier, 2013.

Meanwhile, Ti^{4+} substitution in Ni-rich materials is also helpful in improving structural stability. Recently, Doeff et al. reported improving cycle retention of Ti-substituted $LiNi_{1/3}Co_{1/3}Mn_{1/3}O_2$ and $LiNi_{0.4}Co_{0.2}Mn_{0.4}O_2$ upon cycling to 4.7 V.[16a,37d] They concluded that the stabilization effects of Ti doping came from the substitution of Co^{3+} ions by Ti^{4+} ions, and the valence difference between Co^{3+} and Ti^{4+} is compensated by reduction of Mn^{4+} to Mn^{3+}. Furthermore, Ti substitution can effectively prevent migration of Ni^{2+} from the transition-metal slab to the Li slab leading to suppression of the phase transition in Ni-rich materials.[37b,47]

Mg is a very promising doping element which can realize the "stable pillar effect" in Ni-rich materials, this is because it can substitute Li sites as a result of it having a similar ionic radius to Li^+ ions.[5c,32b] The nickel ion cannot realize the stable "pillar effect" because during cycling it passes through various valence states, which in turn results its ionic radius change during.[16d,20b] Thus, Mg doping can exhibit a greater stable "pillar effect" than Ni doping owing to the constant valence of the magnesium ion during the electrochemical cycles (Figure 11). However, the degree of Li-site substitution

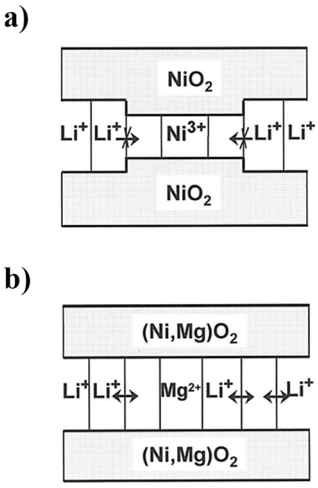

Figure 11. Schematic representation of the inter-slab space.[86] a) In the $Li_xNi_{1+z}O_2$ system, the oxidation of the Ni^{2+} ions during the first electrochemical cycle induces a local collapse of the inter-slab space which makes lithium diffusion and re-intercalation difficult; b) The $Li_xNi_{1-y}Mg_yO_2$ system, the electrochemically inactive Mg^{2+} ions do not hinder lithium diffusion since their size is very close to that of the Li^+ ion. Copyright: the Electrochemical Society, 2000.

of Mg^{2+} is still under debate.[48] Therefore, it is extremely important that find direct evidence of Li site substitution by Mg^{2+} ions by direct atomic resolution analysis, such as scanning transmission electron microscopy (STEM) and electron energy loss spectroscopy (EELS). The doping elements, such as magnesium and nickel, have a pillar effect because they decrease the Li diffusion during charge/discharge.[16f] Accordingly, concentration-gradient materials, which have a higher concentration of doping material at the surface than at the core, are suitable to maximize structural stability and minimize the decrease of power density. Recently epitaxial heterostructure and concentration-gradient materials have been reported.[49] Both these methods improved structural stability of the pristine materials with high lithium diffusivity and electron mobility as a result of the materials having the same oxygen arrangement at the surface and the core. However, heating epitaxial-heterostructure and concentration-gradient materials above 400 °C results in thermal diffusion of metal ions. Therefore, advanced analyses, such as doping elements mapping and certification of doping depth, are needed to understand the doping effect.[49a] In addition, the concentration-gradient and heterostructure materials should be compared with not only pristine materials or core-composition materials but also no concentration gradient materials, which have the same average composition as the concentration gradient materials to ensure there is a surface-stabilization effect compared to the bulk properties.

On the other hand, doping methods with electrochemically active elements, such as Fe and Cr, exhibited limited performances compared to electrochemically inactive elements. For instance, Fe doping of Ni-rich materials results in a decrease of discharge capacity with increasing doping ratio, because iron ions prevent lithium ions diffusing and increases the oxidation potential of nickel ions.[50]

As mentioned above, although significantly different doping effects were reported with different dopants or doping methods, the effect of each dopant and the degree of surface stabilization brought about by the concentration gradient is still unknown (Figure 12). In addition, how the electrochemical properties change with the doping depth clearly need to be verified, too. Therefore, more fundamental studies of the doping effect, doping-depth control, and doping method should be conducted to further aid the development of high-energy LIBs.

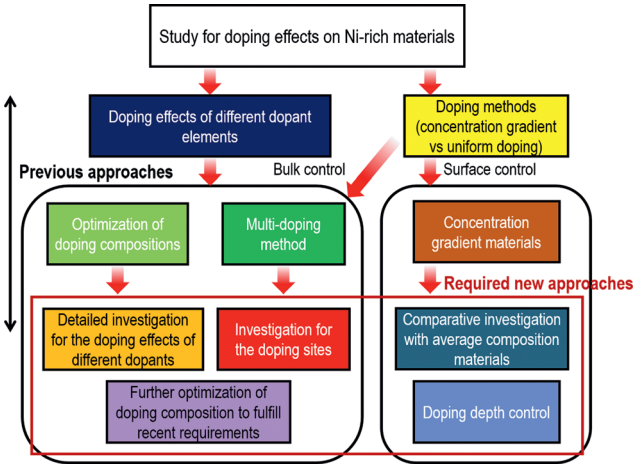

Figure 12. Problems and approaches for doping effects on Ni-rich cathode materials.

4.2. Stabilization of the Solid-Electrolyte Interface

Modifications by substitution or doping are adequate approaches to enhance the electrochemical performances and thermal stabilities of LIBs cathode materials. However, such methods lower both the capacity and power of the active materials. In contrast, applying a coating to the cathode material causes little decrease in capacity because there is almost no decrease of the active components. The interface between electrode and electrolyte is the key area for charge transference, Li^+ diffusion, and side reactions. Engineering the interface through nanoscale coating is an effective method to enhance the electrochemical properties of LIBs, the improvement can be ascribed to modifying the surface chemistry. The major role of the coating layer is as an HF scavenger which consumes acidic molecules and suppresses metal dissolution in organic electrolytes.[8c,51]

4.2.1. Surface-Coating Method

Since Amatucci et al. first modified cathode materials by using a B_2O_3 oxide coating, extensive studies have explored different metal oxides (ZrO_2,[52] Al_2O_3,[53] MgO,[54] SiO_x,[55] etc.) and their coating effects.[56] Cho et al. encapsulated $LiNiO_2$ particles in thin films of zirconium oxide.[52] The thin film encapsulation can effectively suppress the variation of lattice constants during charge/discharge process, thereby alleviating the problems of phase transition (Figure 13 a,b). As a result, the coated $LiNiO_2$ shows a significant improvement in stability over many cycles, as shown in Figure 13 c. Lee et al. also deposited nano-sized ZrO_2 particles on the surface of $LiNi_{0.8}Co_{0.2}O_2$ cathode material, and attributed the improvement to the suppression of impedance growth during cycling rather than suppression of phase transition.[57] These metal oxide coating materials usually act as a protective layer that prevents the cathode material from being exposed directly to the acidic liquid electrolyte. It leads to minimization the harmful side reactions resulting in restraining the exothermic reaction as well as improved electrochemical performance. However, the metal oxide layer also acts as a resistance layer because of its electrochemically and electrically inactive nature.

For this reason, the electron conducting or ion conducting materials, such as carbon and lithium ion conductors, have

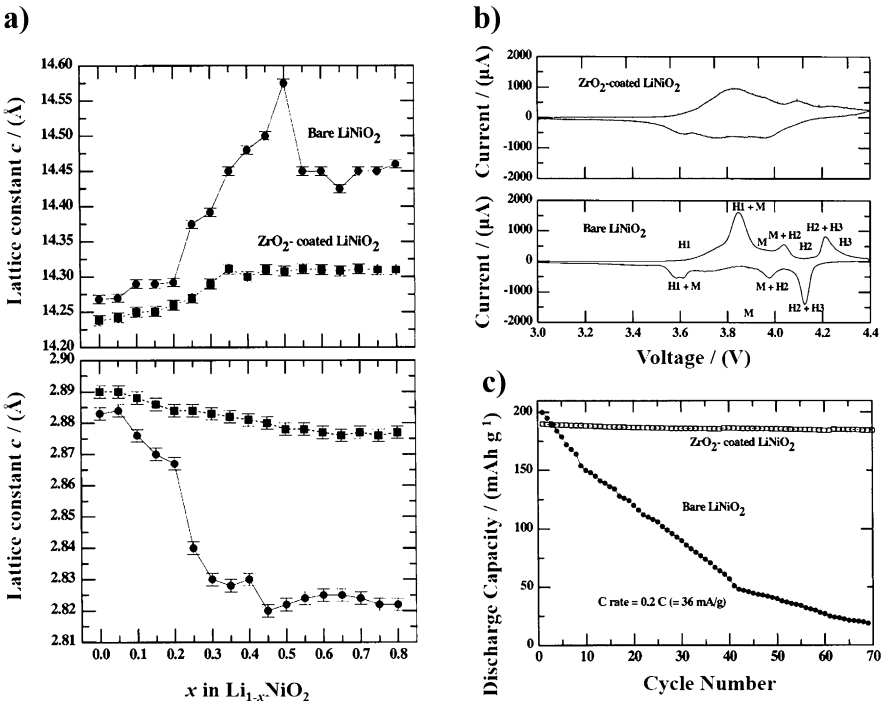

Figure 13. Structure change and electrochemical performance of bare and ZrO_2-coated $LiNiO_2$.[52] a) Evaluation of the lattice constants *a* and *c* as a function of *x* in bare and ZrO_2-coated $Li_{1-x}NiO_2$. b) Cycle stability of bare and ZrO_2-coated $LiNiO_2$ at the rate of 0.2 C. c) Cycle stability of bare and ZrO_2-coated $LiNiO_2$. Copyright: the Electrochemical Society, 2001.

been developed as alternative coating materials. Yoon et al. synthesized a $LiNi_{0.8}Co_{0.15}Al_{0.05}O_2$–graphene composite through a high-energy mechanical ball milling (HEMM) process.[58] When the current density increases up to 10 C and 20 C rates, the $LiNi_{0.8}Co_{0.15}Al_{0.05}O_2$–graphene composite could still deliver a superior capacity of approximately 152 and 112 mAh g^{-1} with stable cycling, values which are almost two times higher than those of the bare cathode. Lithium-ion conductors have also been applied as coating layers on active material surfaces. Ying et al. coated $LiNi_{0.8}Co_{0.2}O_2$ powder with $Li_2O{\cdot}2B_2O_3$ glass through mixing $LiNi_{0.8}Co_{0.2}O_2$, $LiOH{\cdot}H_2O$ and H_3BO_3 together.[59] The resulting $Li_2O{\cdot}2B_2O_3$ glass showed fast Li^+ conductivity and uniform coverage could also be achieved with a minimal amount. The surface modified $LiNi_{0.8}Co_{0.2}O_2$ has a much improved discharge capacity and cycling performance, compared with the bare counterpart, especially at elevated temperature.

In a more advanced approach, coated electrode materials which facilitate both fast Li^+ insertion/delithiation and electron transference have been investigated. In $LiNi_{0.5}Mn_{0.5}O_2$, the average valence of Mn is 4+, so that the electrochemical inert Mn^{4+} can decrease structural instability which leads to outstanding electrochemical cycle performance, even at high voltage. Therefore coating $LiNi_{0.8}Co_{0.1}Mn_{0.1}O_2$ thoroughly with relatively stable $LiNi_{0.5}Mn_{0.5}O_2$ as a "core–shell" structure becomes a reasonable approach to achieve both high capacity and high surface stability. Based on this hypothesis, Sun et al. reported core–shell cathode materials, which achieve both advantages of a high reversible energy density of the core materials and a superior stability of the shell materials, as shown in Figure 14.[60] However, repeated charge/discharge cycles cause voids bigger than 10 nm between the core and shell parts, owing to different stresses endured by the structural mismatch. To mitigate the structural mismatch problem, Sun and Amine et al. developed a concentration gradient strategy.[60c,61] Ni-rich hydroxide with a concentration-gradient shell is achieved by co-precipitation with a gradually changing Ni, Co, and Mn concentration. Heating the hydroxide with the lithium salt results in a concentration-gradient cathode material, which has no structural mismatch at the core and shell interface. However, one disadvantage of the core–shell structure or concentration gradient materials comes from the thick coating shell up to 2 μm, because the thick coating shell limits the rate of electron delivery and Li^+ transportation. In order to address this carrier transportation concern, Ni-based heterostructure cathode materials have been developed in our group (Figure 15). One development is changing the shell material to the spinel structure with three dimensional Li^+ diffusion routes to facilitate easier charge transfer. This Ni-rich cathode material consists of a core material, layered $Li[Ni_{0.54}Co_{0.12}Mn_{0.34}]O_2$ phase ($R\bar{3}m$), and a thin shell of stable $Li_{1+x}[CoNi_xMn_{2-x}]_2O_4$ spinel structure ($Fd\bar{3}m$).[62] The cathode material demonstrates both high energy and high thermal stability, with a high discharge capacity of 200 mAh g^{-1} and 95% capacity retention at 60 °C between 3.0–4.5 V. Moreover, the spinel-layered core–shell structure shows excellent rate capacity and thermal stability. When 10 wt% of a Mn precursor was coated on the $Ni_{0.7}Co_{0.15}Mn_{0.15}(OH)_2$, the final cathode, after calcination, was $LiNi_{0.62}Co_{0.11}Mn_{0.58}O_2$ consisting of a 10 nm thick nanoscale pillar layer on the surface rather than a spinel phase.[22]

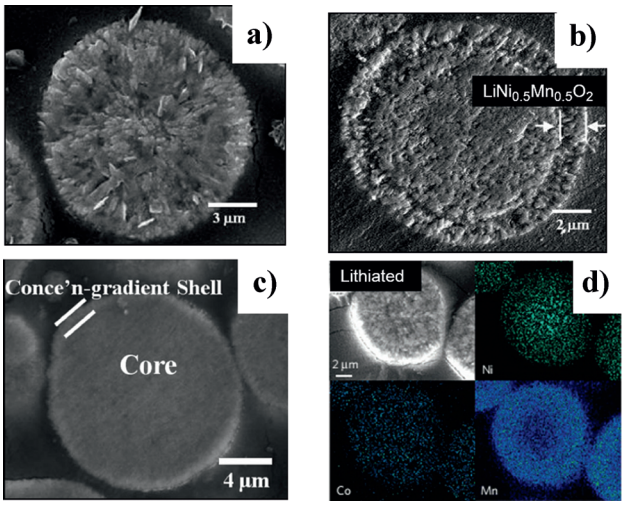

Figure 14. Different types of concentration-gradient "core–shell" Ni-rich cathode materials. a) Cross-sectional image of a $Li(Ni_{0.8}Co_{0.1}Mn_{0.1})O_2$ particle.[60b] Copyright: American Chemical Society, 2006. b) core–shell $Li(Ni_{0.8}Co_{0.1}Mn_{0.1})O_2$-$Li(Ni_{0.5}Mn_{0.5})O_2$.[60a] Copyright: American Chemical Society, 2005; c) Concentration gradient $Li(Ni_{0.72}Co_{0.18}Mn_{0.1})O_2$.[61c] Copyright: Nature Publishing Group, 2009. d) Full concentration-gradient $Li(Ni_{0.75}Co_{0.1}Mn_{0.15})O_2$.[61a] Copyright: Nature Publishing Group, 2012.

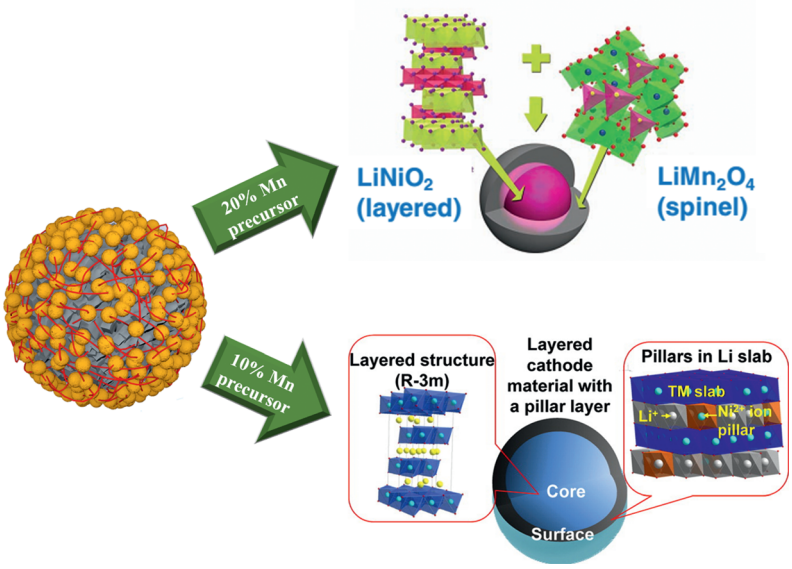

Figure 15. Schematic view of hetero-structure core–shell cathode materials. In the core–shell structure, the shell material consists of either a spinel structure[62] (top; Copyright: Wiley-VCH, 2011) or a rock salt phase (bottom)[22] depending on the synthetic method. Copyright: American Chemical Society, 2013.

Note that substitution of Ni ions in Ni-baseed materials by Mn ions increases generation of Ni^{2+}. As mentioned in section 3.1., the Ni^{2+} ions tend to migrate into the Li site, simultaneously. Thus, the Ni^{2+} pillared Li slabs exist as an thin cation mixed layer on the surface of the Ni-rich cathode, and the transition-metal migration resulted in a rock salt phase with $Fm\bar{3}m$ space group. When the nanoscale rock salt has been introduced into the cathode, the cycle performance at 60 °C with 4.5 V cutoff voltage was significantly improved and the amount of heat generation was drastically reduced to 167 $J g^{-1}$. Therefore, the nano-scale pillar layer was shown to contribute to improving structural stability at elevated temperatures.

4.2.2. *A Promising Coating Method: Lithium Reactive Coating*

Ni-based cathode materials have a strong tendency to take up moisture and they have a high concentration of residual impurities such as Li_2CO_3 and LiOH. These residual surface species cause the cathode slurry to form a gel leading to irregular coating thickness and insufficient adhesion on current collector. Other problems include severe gas evolution and deposition of insulating LiF from the decomposition of the surface impurities and electrolyte. During the coating process, surface residual LiOH and Li_2CO_3 dissolve into the water and then re-precipitate on the coating surface of cathode materials. These impurities remain even after annealing at 700 °C and are expected to result in gas generation during storage at 90 °C. However, the surface chemistry of the cathode materials can be changed by lithium reactive coating as shown in Figure 16.

Previous work revealed that $AlPO_4$ nanoparticles can react with residual lithium species during heat treatment at 700 °C, and produce Al-rich $LiAl_yCo_{1-y}O_2$ and P-rich Li_3PO_4 regions on the active material surface. Not only does this decrease the amount of residual lithium species on the surface but the combination Li_3PO_4, which is a Li^+ conductor, and the Al-doped $LiMO_2$ phase contribute to a remarkably improved cycling performance relative to bare cathode material.[63] As expected, $AlPO_4$ coated-$LiNi_{0.8}Co_{0.1}Mn_{0.1}O_2$ improved both thermal stability and electrochemical properties.[64] The concentrations of Co and Ni dissolved in the electrolyte after cycling were 80 and 20 ppm, with negligible Mn ion dissolution. Clearly the surface $AlPO_4$ layer suppresses metal-ion dissolution which would otherwise arise from attack by HF from the electrolyte.

The $AlPO_4$ coating layer also minimizes the exothermic reaction of the de-lithiated cathode material, it is this exothermic reaction which triggers the "thermal runaway" of LIBs.[65] Cells with the $AlPO_4$-coated $LiNi_{0.8}Co_{0.1}Mn_{0.1}O_2$ cathode did not exhibit thermal runaway. Cho et al. also demonstrated the overcharge (12 V) behavior of the $AlPO_4$ coated $LiCoO_2$ and $LiNi_{0.8}Co_{0.1}Mn_{0.1}O_2$ in terms of exothermic reactions. The surface temperature of the cell using $AlPO_4$-coated $Li_xNi_{0.8}Co_{0.1}Mn_{0.1}O_2$ as the cathode did not exceed 125 °C, while the cell with coated Li_xCoO_2 exceeded 170 °C.[66] The effectiveness of using $AlPO_4$ as a coating material has also been confirmed by other scientists. Zeng et al.[67] have investigated the $AlPO_4$ coating effect on $LiNi_{0.8}Co_{0.2}O_2$ particles with 90 °C storage for 4 h, and found that the surface structure of bare and $AlPO_4$-coated $LiNi_{0.8}Co_{0.2}O_2$ particles showed different phase transformations. As a result, the layered structure of bare material was changed to a NiO rock salt phase ($Fm\bar{3}m$) at the surface, while the $AlPO_4$ coated sample transformed to a spinel-like phase with less loss of oxygen. Ma et al. also coated $AlPO_4$ on $LiNi_{0.8}Co_{0.2}O_2$ cathodes at 550 °C for 5 h in furnace.[68] The HRTEM image showed an evenly distributed coating layer on the bare material. The main mechanism of improvement after $AlPO_4$ coating is principally assigned to minimizing harmful side reactions by forming a protective layer at the interface between active material and electrolyte. Cho et al. revealed that $Co_3(PO_4)_2$ could also consume surface impurities during annealing to form a uniform coating layer on the bulk surface.[69] The residual Li species and $Co_3(PO_4)_2$ nanoparticles reacted completely with each other at 700 °C, thus forming lithium-deficient olivine Li_xCoPO_4. The olivine coating layer is expected to improve both the electrochemical performance and thermal stability of the $LiNi_{0.8}Co_{0.16}Al_{0.04}O_2$ cathode material as a result of the olivine phase's highly electrochemical and thermal stability. This surface-coated sample has a 30 % enhancement of the cycle life compared to that of the bare cathode material. Storage test of the 4.3 V charged electrode at 90 °C after 7 days showed that the bare sample transformed into spinel phase with a $Fd\bar{3}m$ space group, whereas the $Co_3(PO_4)_2$-coated sample remains as a layered hexagonal phase with $R\bar{3}m$ space group. Further investigation of the effect of concentration and annealing temperature of Li_xCoPO_4 reveals that the P atoms remain on the particle surface even after annealing at 700 °C for 7 h.[70] The sample sintered at 700 °C for 7 h had a decreased total heat capacity of 240 $J g^{-1}$, which is much smaller than the bare material (980 $J g^{-1}$). Ryu et al. also confirmed that the $Co_3(PO_4)_2$ nanoparticles effectively reacted with surface impurities such as Li_2CO_3, and that after calcination

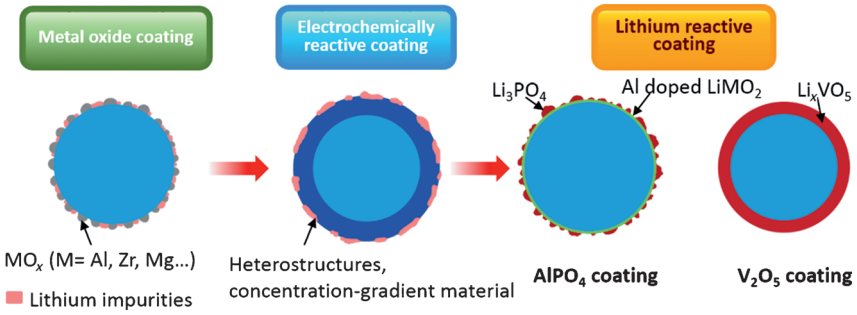

Figure 16. Different coating strategies. Metal oxides and materials with electrochemically active materials coatings have lithium impurities remaining on the surface. On the other hand, materials with lithium reactive coatings consume residual lithium species: $AlPO_4$ on the surface reacts with residual lithium impurities forming Li_3PO_4, the Al doping layer, $Co_3(PO_4)_2$, converts into a uniform Li_xCoPO_4 coating layer.

the surface residues could no longer be detected by TEM analysis.[71]

To further improve the electronic and Li^+ conductivity of the surface coating layer, we recently tried to coat the particle surface with V_2O_5 to get a multi-shell coating configuration (Figure 17).[72] NH_4VO_3 was used as a coating precursor,

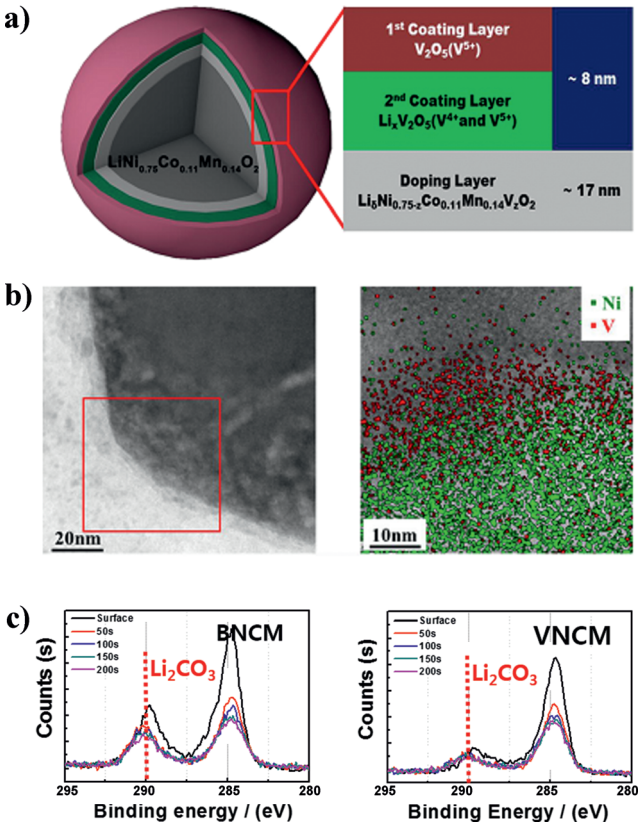

Figure 17. Schematic representation of a multi-shell coated Ni-rich cathode material and its coating effect.[88] a) The V_2O_5 modified $LiNi_{0.75}Co_{0.11}Mn_{0.14}O_2$ cathode material with multi-shell surface structure; b) Cross-sectional TEM image of the V_2O_5 coated Ni-rich cathode material, and corresponding EELS spectra of the distribution of V and Ni. c) XPS spectra of bare (BNCM) and V_2O_5-coated (VNCM) Ni-rich cathode material, which demonstrates consumption of surface lithium species. Copyright: American Chemical Society, 2014

because ionized VO^{3-} can react with Li^+ ions from LiOH and Li_2CO_3 on the particle surface. This coating method resulted in multi-shelled layers including V_2O_5-$Li_xV_2O_5$-$LiNi_{0.75-z}Co_{0.11}Mn_{0.14}V_zO_2$ in the final cathode particle after annealing at 400 °C. The V_2O_5-$Li_xV_2O_5$ surface layers support a significantly improved fast charge capability of the cathode. Furthermore, such lithium-consuming coating layers prevent side reactions with moisture in air and the electrolyte and also provide stable cycle performance even at 60 °C.

To sum up, surface coating is an effective way to improve the Ni-rich materials' structural and electrochemical stability, although the exact mechanism by which the surface coating functions is still the subject of controversy.[73] Rough coating with metal oxides as HF scavengers has been confirmed to improve the cycle stability of lithium-ion cells at room temperature, while the long term cycling at elevated temperature (60 °C) needs to be further addressed in a comprehensive way. The lithium reactive coating of $Co_3(PO_4)_2$, which can consume residual lithium species on the surface of Ni-rich cathode materials thus forming a Li_xCoPO_4 coating layer, shows the best cycle stability and safety characteristics at 60 °C. However, it is still a big challenge to understand the composition and structure of the coating layer and their interaction with bulk and electrolyte. Therefore, some cutting edge surface analysis techniques such as XAS, HRTEM–EELS, TOF–SIMS, and in situ spectroscopies should be further employed to gain more understanding of the surface composition, structure deterioration, and their implication with electrochemical performance and safety.

5. Remaining Challenges

5.1. Safety Issue

High-capacity lithium-ion batteries in a charged state can be very dangerous if exothermic reactions start between the active materials and organic electrolytes. One of the most serious problems of the Ni-rich materials is their thermal instability that would cause severe safety problems during thermal runaway. The triggering mechanism is related to the cathode structural instability, which results in oxygen release. For instance, in Li_xNiO_2, for x values less than 0.25, exothermic reactions with the electrolytes begin at around 200 °C (the onset temperature). Consequently, the heat generated from reactions between the de-lithiated cathode and the electrolytes, may lead to very dangerous situations. These reactions will generate lots of gas and heat and lead to a sharp inner temperature rise, increasing pressure, and finally explosion of the batteries. In particular, the oxygen species released from the cathode framework are so reactive with the electrolytes that they contribute greatly to the thermal runaway. Therefore, the safety of lithium-ion batteries can be greatly improved by inhibiting the oxygen evolution, and thus decreasing the heat generation and delaying the time taken to reach the onset temperature of the exothermic reactions.

The evolution of both O_2 and CO_2 gases is caused by phase changes from the layered structure ($R\bar{3}m$) to the disordered spinel structure ($Fd\bar{3}m$) and the rock salt structure ($Fm\bar{3}m$)[45c] (Figure 18a–c). According to the K-edge XANES and EXAFS data of nickel and cobalt atoms in $Li_{0.5}Ni_{0.8}Co_{0.15}Al_{0.05}O_2$, stable phases in the de-lithiated state for each transition-metal element are different. Nickel ions can be stabilized in the NiO rock-salt structure, while cobalt ions easily form the Co_3O_4 spinel-like structure when the temperature is not high enough to form the rock-salt structure.[45c] The state of charge has a great impact on both the phase transition and the oxygen evolution. As the degree of de-lithiation increases, the onset temperature of the structural change decreases and the amount of oxygen evolution increases.

Hwang et al. studied the local evaluation of the surface structure of $Li_xNi_{0.85}Co_{0.15}Al_{0.05}O_2$ as a function of the state of

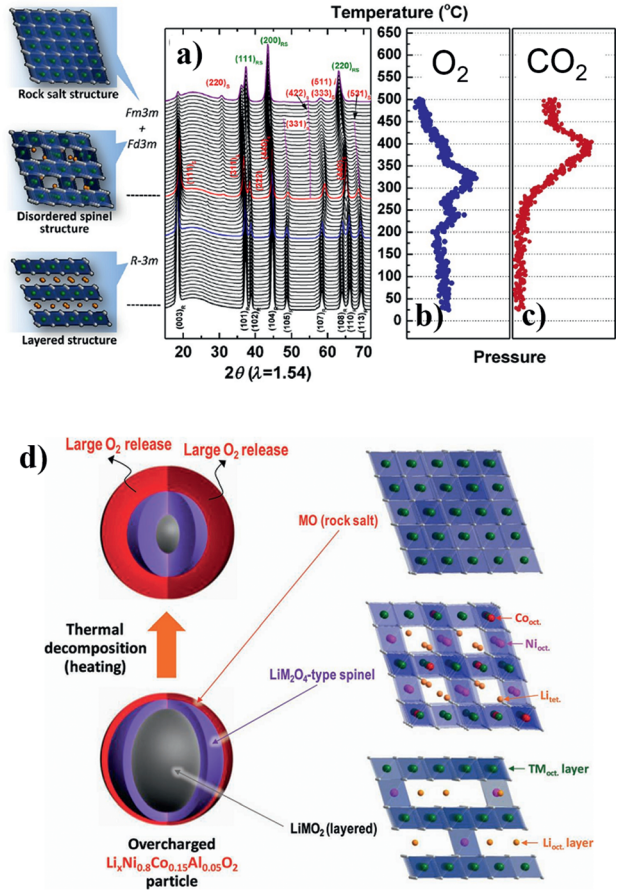

Figure 18. a) TR-XRD patterns and simultaneously measured mass spectra (MS) for b) O_2 and c) CO_2, released from $Li_{0.5}Ni_{0.8}Co_{0.15}Al_{0.05}O_2$ during heating to 500 °C.[45c] Copyright: American Chemical Society, 2013. d) Schematic representation of the thermal decomposition of the overcharged $Li_xNi_{0.8}Co_{0.15}Al_{0.05}O_2$ cathode during heating, in which the phase change propagates from the surface to core of the overcharged particle.[89] Copyright: Wiley-VCH, 2013.

charge ($0.1 \le x \le 0.5$) using TEM and EELS.[74] Structural changes start on the surface as soon as the charge process leads to a lower lithium content or more lithium vacancies at the outer part of the particle. Wu et al. described the overcharged $Li_xNi_{0.85}Co_{0.15}Al_{0.05}O_2$ as a core–shell surface structure with a layered-structure core, spinel-structure shell, and a rock-salt-structure surface.[75] Furthermore, the complex microstructures were converted into a single NiO rock salt phase after the heat process, resulting in capacity and rate performance fade of electrodes (Figure 18d). As discussed in Section 4.2., the incorporation of Mn^{4+} and Al^{3+} can effectively stabilize the layered structure, and was confirmed to postpone the onset temperature of exothermic reactions. Mg^{2+} doping into $LiMO_2$ compounds can also effectively enhance the thermal stability. This doping effect may be due to the pillar effect of the electrochemical inactive ions in the Li slab, which can effectively eliminate the phase transition in the charged state.

The effects of electrolyte decomposition products on the pristine and TiO_2-coated $Li_{1-x}Ni_{0.8}Co_{0.2}O_2$ ($1 > x > 0$) cathode materials have been investigated by thermal analytical and temperature-programmed desorption-mass spectroscopy (TPD-MS) techniques.[76] From the data, we can easily recognize that the thermal stability of the active material is heavily dependent on the by-products from direct and indirect electrolyte oxidation, such as carboxylates. Those by-products attach to the surfaces of the de-lithiated particles and accelerate the thermal decomposition reactions of the materials. The positive effect of the coating method on the thermal stability can be interpreted in two different ways. The first one is suppression of electrolyte decomposition and a decrease in the amount of undesired by-products attached to the surface of the electrode surface. The second coating effect is forming a more stable surface, which can reduce the formation of seeds for cation mixing phase. Thus, surface coating can inhibit not only the formation of by-products from electrolyte decomposition reactions but also the spread of cation disordered-phases.

Although intensive studies monitoring the structural changes and heat generation during thermal decomposition have resulted in great progress in this area, the detailed correlation between structural changes and oxygen evolution is still not clear. Accordingly, further understanding of the structural deterioration and doping/coating effect is needed.

5.2. Microstrain and Crack of Primary Particles

The deterioration of the Ni-rich cathode has usually been assigned to the degradation of the layered structure, the rise of cell impedance, and the formation of a film on the surface cathode, the film being a mixture of LiF, MF_n, polycarbonates, Li_xPF_y-type, and $Li_xPF_yO_z$-type compounds. However, in addition, it has also been emphasized recently that significant capacity loss is caused by numerous microcracks generated in the Ni-rich particles.

Huang et al. used STEM to compare single-cycled $LiNi_{0.8}Co_{0.15}Al_{0.05}O_2$ (NCA) particles with pristine spherical powders to reveal the degradation mechanism of Ni-rich cathodes.[77] The NCA particle (secondary particle) prepared by co-precipitation consists of small aggregated grains (primary particles) under 1 μm in diameter with micro-voids along the grain boundaries. With only one cycle, some micro-cracks can be observed at triple junctions (where three primary particles touch) and grain boundaries. Moreover, the thicker grain boundary layers and micro-cracks are more frequent near the surface of large particles or in small particles. In the core–shell Ni-rich cathode materials, repeated charge/discharge cycling caused voids larger than 10 nm to form between the core and shell materials, owing to different stresses endured because of structural mismatch.[60a] The Ni-rich core material ($Li[Ni_{0.8}Co_{0.1}Mn_{0.1}]O_2$) tends to undergo a volume change of approximately 9–10% while the shell material ($Li[Ni_{0.5}Mn_{0.5}]O_2$) only shrinks by about 3% during de-intercalation. Lee et al. also observed numerous voids inside concentration-gradient Ni-rich particles after 2500 cycles, there were even large cracks throughout the whole particle when cycled between 2.7–4.5 V at 55 °C.[78] The electrochemical-cycling-induced microstrain and particle fracture have also been observed in cycled $LiCoO_2$ (LCO)

particles.[79] Cycling only 50 times of between 2.5–4.35 V can cause severe internal strain and dislocation defects in crystal grains of LCO. Several possible mechanisms have been proposed for the strain damage. The stresses can arise from anisotropic lattice expansion and contraction upon Li^+ extraction/insertion, which cause volume variation of the grains.[80] The individual grains in a sintered secondary particle are physically constrained by their neighboring primary particles and stress arising from the anisotropic volume change can cause particle fracture in long term cycle. The differential expansion within a single grain can also contribute to microstrain because a Li^+ concentration gradient always exists in a primary particle during charge–discharge process. Another possibility for such crack formation is strongly related to the uneven Li^+ concentration and cation disorder. When the Li^+ concentration is locally over-depleted, it results in a phase transformation to spinel and NiO-type rock salt phases. The crystal structure mismatch between the $R\bar{3}m$ layered structure and undesired phases, such as spinel and rock salt phase, leads to severe microstrain within a primary particle during repeated charge–discharge.

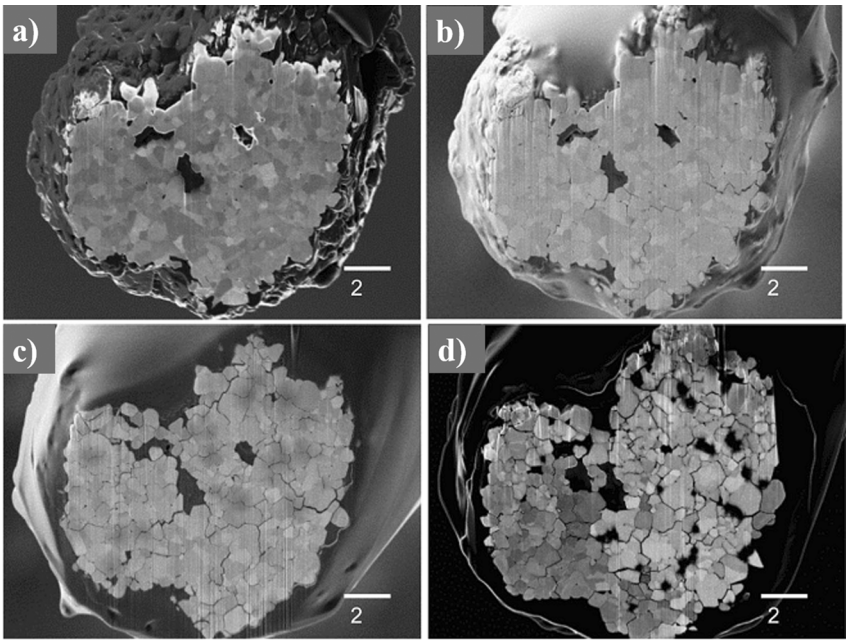

Figure 19. Scanning electron microscope images showing the progression of $LiNi_{0.8}Co_{0.15}Al_{0.05}O_2$ particle fracture and fragmentation as a function of cycle using the snapshot approach.[81] These images show the same particle in the a) as prepared condition and after b) one, c) two, and d) three complete charge/discharge cycles. Copyright: Wiley-VCH, 2013.

To directly investigate the correlation between microstructure evolution and electrochemical processes, Miller et al. developed a micro-battery setup for in situ SEM observation of single Ni-rich particles during electrochemical cycling (Figure 19).[81] The micro-crack and inter-grain separation developed at the cathode active materials during a first delithiation process with high *C*-rate and electrolyte could permeate into the particle interior through the crack network. These cracks caused loss of inner particle connectivity and give rise to increased polarization, which contributed to the degradation of performance and capacity fade. Wantanabe et al. investigated the cycle deterioration of Li-ion cells with NCA under different depths of discharge (DOD) and different temperatures.[82] In their study, the micro-crack generation and growth heavily depended on the conditions of charge–discharge, as shown in Figure 20.[79b] For the cycle test in 100% DOD, micro-cracks are easily generated inside the particles because of the large lattice mismatch between the contraction and the expansion with an approximately 3% volume change because the oxygen framework cannot cope with such a change. The electrolyte infiltration into the interior of the secondary particle along the micro-crack network occurs and causes the formation of a thick SEI film and formation of a NiO-phase at the grain boundaries. Generation of voids and surface microstructure changes cause poor electrical contact between the primary particles and lead to capacity and power deterioration. On the other hand, almost no cracks evolved with 60% DOD even after 5000 cycles. The formation of NiO-phases and SEI compounds only occurred at the surface of secondly particles. Therefore, suppression of microstrain and preventing failure of the primary particle are of critical importance in achieving prolonged cycling stability especially at high temperature. In our group, we have found that the nanoscale surface pillar layer is effective at suppressing primary particle fracture during cycling at 60 °C.[22] Further engineering of the surface microstructure of the primary particles through coating or surface doping may be a valuable strategy to give

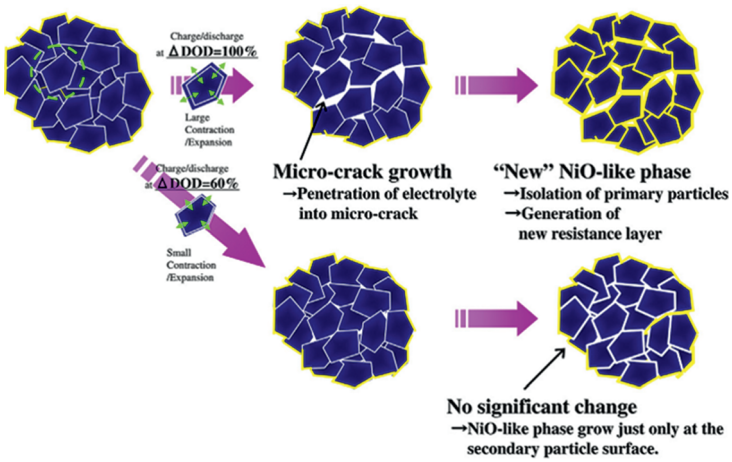

Figure 20. A schematic model for the micro-crack growth and deterioration of a $LiNi_{0.76}Co_{0.14}Al_{0.10}O_2$ particle during cycle tests.[82] Copyright: Elsevier, 2014.

excellent cycle life by reducing the volume expansion of grains and suppressing the generation of micro-cracks.

6. Summary and Outlook

Layered lithium Ni-rich compounds $LiNi_{1-x}M_xO_2$ ($0.1 < x < 0.5$) have been taken into account as promising positive electrode materials for the next generation LIBs with high energy density for large scale application in hybrid electric vehicles or electric vehicles. In comparison to Li-rich cathode materials, they have a relatively large capacity ($< 200\ mAh\,g^{-1}$) and comparably high operating voltage and are more accessible owing to their high rate capability, suitable operating voltage, and high energy efficiency. LIBs with $LiNi_{0.8}Co_{0.15}Al_{0.05}O_2$ (NCA) cathode material have already been used in Tesla for electric vehicle application. When Ni-rich cathode materials are paired with superior Si/C anode materials, a battery with an energy density higher than $250\ Wh\,kg^{-1}$ can be achieved. As far as we know, this lithium ion battery approach is the most accessible high energy-density storage device, which could also have high cycle stability and safety properties.

However, cation disordering between transitional-metal sites and lithium sites gives rise to structural instability and sluggish Li^+ diffusion. Surface side reactions usually happen both in air and electrolyte, and cause substantial capacity and power loss. Structural instability in the highly de-lithiated state is always a safety concern, which may lead to oxygen release and thermal runaway. Furthermore, for practical applications the volumetric energy density is also important, which needs to be further addressed to increase the useful energy density in the restricted space.

For the last 20 years, continuous efforts have been poured into the chemistry of these cathode materials to understand and improve the structure and electrochemical performance. There are numerous examples of material design based on the understanding of structure–property relationships and thus accelerate the pace of development of high energy-density LIBs. Through the integration of different elements, the structural stability during repeated charge–discharge cycles and the structural stability of the highly de-lithiated state has been substantially improved. Substitution with Co^+ ions can effectively suppress the cation disordering of Ni-based material, leading to enhanced rate capability. Substitutions with Al and Mn ions can be very helpful in stabilizing the layered structure and improving the thermal characteristics. The dopant optimization, doping method, doping depth control are critical to performance and need further understanding and novel approaches. The understanding of the surface chemistry of the electrode is at the core of research and development in LIBs. Strategies for surface modification have evolved from metal oxide coating through functional coating and electrochemical active material coating to lithium reactive coating. Through the lithium reactive material coating, the side reactions of the electrode can be significantly reduced. However, investigations into the surface composition and the microstructure change are necessary to understand the coating effect and further benefit material design.

In summary, the structure/surface properties and performance of Ni-rich cathode materials have been better understood and improved greatly these years. Certainly, these lithium Ni-rich oxides still have many remaining challenges related to structural instability, surface side reactions, and safety concerns. Even so, through continuous scientific efforts, the particle energy density and reliability of this type of cathode material can reach a level suitable for applications and partially relieve the "range anxiety" of electronic vehicles in the future.

This work was supported by the IT R&D program of MOTIE/KEIT (Development of Li-rich Cathode and Carbon-free Anode Materials for High Capacity/High Rate Lithium Secondary Batteries, 10046309).

How to cite: *Angew. Chem. Int. Ed.* **2015**, *54*, 4440–4457
Angew. Chem. **2015**, *127*, 4518–4536

[1] a) J. Liu, J.-G. Zhang, Z. Yang, J. P. Lemmon, C. Imhoff, G. L. Graff, L. Li, J. Hu, C. Wang, J. Xiao, G. Xia, V. V. Viswanathan, S. Baskaran, V. Sprenkle, X. Li, Y. Shao, B. Schwenzer, *Adv. Funct. Mater.* **2013**, *23*, 929–946; b) B. Dunn, H. Kamath, J. M. Tarascon, *Science* **2011**, *334*, 928–935.

[2] M. M. Thackeray, C. Wolverton, E. D. Isaacs, *Energy Environ. Sci.* **2012**, *5*, 7854–7863.

[3] a) B. C. Melot, J. M. Tarascon, *Acc. Chem. Res.* **2013**, *46*, 1226–1238; b) J. B. Goodenough, *Acc. Chem. Res.* **2013**, *46*, 1053–1061; c) J. M. Tarascon, M. Armand, *Nature* **2001**, *414*, 359–367; d) M. Armand, J. M. Tarascon, *Nature* **2008**, *451*, 652–657.

[4] a) B. Xu, D. Qian, Z. Wang, Y. S. Meng, *Mater. Sci. Eng. R* **2012**, *73*, 51–65; b) T.-H. Kim, J.-S. Park, S. K. Chang, S. Choi, J. H. Ryu, H.-K. Song, *Adv. Energy Mater.* **2012**, *2*, 860–872; c) V. Etacheri, R. Marom, R. Elazari, G. Salitra, D. Aurbach, *Energy Environ. Sci.* **2011**, *4*, 3243–3262.

[5] a) P. He, H. J. Yu, D. Li, H. S. Zhou, *J. Mater. Chem.* **2012**, *22*, 3680–3695; b) O. Tsutomu, J. B. Ralph, *J. Power Sources* **2007**, *174*, 449–456; c) C. Delmas, M. Menetrier, L. Croguennec, I. Saadoune, A. Rougier, C. Pouillerie, G. Prado, M. Grune, L. Fournes, *Electrochim. Acta* **1999**, *45*, 243–253.

[6] L. Wang, J. Li, X. He, W. Pu, C. Wan, C. Jiang, *J. Solid State Electrochem.* **2009**, *13*, 1157–1164.

[7] a) Y. Koyama, H. Arai, I. Tanaka, Y. Uchimoto, Z. Ogumi, *Chem. Mater.* **2012**, *24*, 3886–3894; b) H. J. Yu, Y. M. Qian, M. R. Otani, D. M. Tang, S. H. Guo, Y. B. Zhu, H. S. Zhou, *Energy Environ. Sci.* **2014**, *7*, 1068–1078.

[8] a) D. Aurbach, *J. Power Sources* **2003**, *119–121*, 497–503; b) K. Edström, T. Gustafsson, J. Thomas, *Electrochim. Acta* **2004**, *50*, 2–3; c) S. T. Myung, K. Amine, Y. K. Sun, *J. Mater. Chem.* **2010**, *20*, 7074–7095.

[9] T. M. Bandhauer, S. Garimella, T. F. Fuller, *J. Electrochem. Soc.* **2011**, *158*, R1–R25.

[10] See Ref. [5b].

[11] A. Manthiram, A. Vadivel Murugan, A. Sarkar, T. Muraliganth, *Energy Environ. Sci.* **2008**, *1*, 621–638.

[12] K. K. Lee, K. B. Kim, *J. Electrochem. Soc.* **2000**, *147*, 1709–1717.

[13] T. Ohzuku, A. Ueda, M. Nagayama, Y. Iwakoshi, H. Komori, *Electrochim. Acta* **1993**, *38*, 1159.

[14] C. Delmas, L. Croguennec, *MRS Bull.* **2002**, *27*, 608–612.

[15] a) H. Arai, S. Okada, H. Ohtsuka, M. Ichimura, J. Yamaki, *Solid State Ionics* **1995**, *80*, 261–269; b) W. Li, J. N. Reimers, J. R. Dahn, *Solid State Ionics* **1993**, *67*, 123–130; c) J. P. Peres, F. Weill, C. Delmas, *Solid State Ionics* **1999**, *116*, 19–27; d) C. Keke, H. Bengt, M. Denis, *CALPHAD Comput. Coupling Phase Diagrams Thermochem* **2012**, *37*, 100–107.

[16] a) F. Lin, I. M. Markus, D. Nordlund, T. C. Weng, M. D. Asta, H. L. Xin, M. M. Doeff, *Nat. Commun.* **2014**, *5*, 3529; b) L. Cai, Z. C. Liu, K. An, C. D. Liang, *J. Electrochem. Soc.* **2012**, *159*, A924 – A928; c) X. Y. Zhang, W. J. Jiang, A. Mauger, R. Qilu, F. Gendron, C. M. Julien, *J. Power Sources* **2010**, *195*, 1292 – 1301; d) H. H. Li, N. Yabuuchi, Y. S. Meng, S. Kumar, J. Breger, C. P. Grey, Y. Shao-Horn, *Chem. Mater.* **2007**, *19*, 2551 – 2565; e) Y. Hinuma, Y. S. Meng, K. S. Kang, G. Ceder, *Chem. Mater.* **2007**, *19*, 1790 – 1800; f) K. Kang, G. Ceder, *Phys. Rev. B* **2006**, *74*, 094105; g) Y. M. Choi, S. I. Pyun, S. I. Moon, *Solid State Ionics* **1996**, *89*, 43 – 52; h) J. N. Reimers, W. Li, J. R. Dahn, *Phys. Rev. B* **1993**, *47*, 8486 – 8493; i) J. R. Dahn, U. von Sacken, C. A. Michal, *Solid State Ionics* **1990**, *44*, 87 – 97.

[17] a) B. Zhang, L. J. Li, J. C. Zheng, *J. Alloys Compd.* **2012**, *520*, 190 – 194; b) Z. L. Huang, J. Gao, X. M. He, J. J. Li, C. Y. Jiang, *J. Power Sources* **2012**, *202*, 284 – 290.

[18] J. Lee, A. Urban, X. Li, D. Su, G. Hautier, G. Ceder, *Science* **2014**, *343*, 519 – 522.

[19] a) C. Yu, G. S. Li, X. F. Guan, J. Zheng, L. P. Li, *Electrochim. Acta* **2012**, *61*, 216 – 224; b) P. Gao, Y. H. Li, H. D. Liu, J. Pinto, X. F. Jiang, G. Yang, *J. Electrochem. Soc.* **2012**, *159*, A506 – A513; c) C. X. Cheng, L. Tan, H. W. Liu, X. T. Huang, *Mater. Res. Bull.* **2011**, *46*, 2032 – 2035.

[20] a) S.-K. Jung, H. Gwon, J. Hong, K.-Y. Park, D.-H. Seo, H. Kim, J. Hyun, W. Yang, K. Kang, *Adv. Energy Mater.* **2014**, *4*, 1300787; b) A. Boulineau, L. Simonin, J. F. Colin, C. Bourbon, S. Patoux, *Nano Lett.* **2013**, *13*, 3857 – 3863.

[21] R. Huang, Y. Ikuhara, *Curr. Opin. Solid State Mater. Sci.* **2012**, *16*, 31 – 38.

[22] Y. Cho, P. Oh, J. Cho, *Nano Lett.* **2013**, *13*, 1145 – 1152.

[23] R. V. Chebiam, F. Prado, A. Manthiram, *J. Solid State Chem.* **2002**, *163*, 5 – 9.

[24] X. Lu, Y. Sun, Z. Jian, X. He, L. Gu, Y.-S. Hu, H. Li, Z. Wang, W. Chen, X. Duan, L. Chen, J. Maier, S. Tsukimoto, Y. Ikuhara, *Nano Lett.* **2012**, *12*, 6192 – 6197.

[25] a) J. N. Reimers, J. R. Dahn, *J. Electrochem. Soc.* **1992**, *139*, 2091 – 2097; b) G. G. Amatucci, J. M. Tarascon, L. C. Klein, *J. Electrochem. Soc.* **1996**, *143*, 1114 – 1123.

[26] a) J. G. Chen, B. D. Vries, J. T. Lewandowski, R. B. Hall, *Catal. Lett.* **1994**, *23*, 25 – 35; b) T. Nohma, H. Kurokawa, M. Uehara, M. Takahashi, K. Nishio, T. Saito, *J. Power Sources* **1995**, *54*, 522 – 524; c) C. C. Chang, N. Scarr, P. N. Kumta, *Solid State Ionics* **1998**, *112*, 329 – 344.

[27] a) See Ref. [15a]; b) See Ref. [13].

[28] a) D. H. Cho, C. H. Jo, W. Cho, Y. J. Kim, H. Yashiro, Y. K. Sun, S. T. Myung, *J. Electrochem. Soc.* **2014**, *161*, A920 – A926; b) D. Aurbach, Y. Eineli, B. Markovsky, A. Zaban, S. Luski, Y. Carmeli, H. Yamin, *J. Electrochem. Soc.* **1995**, *142*, 2882 – 2890.

[29] A. M. Andersson, D. P. Abraham, R. Haasch, S. MacLaren, J. Liu, K. Amine, *J. Electrochem. Soc.* **2002**, *149*, A1358 – A1369.

[30] G. V. Zhuang, G. Y. Chen, J. Shim, X. Y. Song, P. N. Ross, T. J. Richardson, *J. Power Sources* **2004**, *134*, 293 – 297.

[31] C. H. Chen, J. Liu, K. Amine, *J. Power Sources* **2001**, *96*, 321 – 328.

[32] a) M. S. Whittingham, *Chem. Rev.* **2004**, *104*, 4271 – 4301; b) Y. P. Wu, E. Rahm, R. Holze, *Electrochim. Acta* **2002**, *47*, 3491 – 3507; c) J. D. Wilcox, E. E. Rodriguez, M. M. Doeff, *J. Electrochem. Soc.* **2009**, *156*, A1011 – A1018; d) J. Wilcox, S. Patoux, M. Doeff, *J. Electrochem. Soc.* **2009**, *156*, A192 – A198; e) J. Kim, K. Amine, *J. Power Sources* **2002**, *104*, 33 – 39; f) T. Ohzuku, A. Ueda, M. Nagayama, *J. Electrochem. Soc.* **1993**, *140*, 1862 – 1870; g) I. H. Kwon, H. R. Park, Y. Y. Song, *Russ. J. Electrochem.* **2013**, *49*, 221 – 227; h) M. Y. Song, C. K. Park, H. R. Park, D. R. Mumm, *Electron. Mater. Lett.* **2012**, *8*, 37 – 42; i) M. Y. Song, D. R. Mumm, C. K. Park, H. R. Park, *Met. Mater. Int.* **2012**, *18*, 465 – 472; j) M. Y. Song, D. S. Lee, H. R. Park, *Mater. Res. Bull.* **2012**, *47*, 1021 – 1027; k) H. U. Kim, J. H. Song, D. R. Mumm, M. Y. Song, *Ceram. Int.* **2011**, *37*, 779 – 782; l) H. R. Park, *J. Ind. Eng. Chem.* **2010**, *16*, 698 – 702; m) S. Kwon, S. D. Yoon, H. Park, M. Song, *Ceram. Int.* **2010**, *36*, 893 – 898; n) M. Y. Song, S. N. Kwon, S. D. Yoon, D. R. Mumm, *J. Appl. Electrochem.* **2009**, *39*, 807 – 814; o) M. Song, S. Kwon, H. Park, *Ceram. Int.* **2009**, *35*, 3135 – 3142; p) S. Myoung Youp, K. Sung Nam, Y. Soon-Do, R. M. Daniel, *J. Appl. Electrochem.* **2008**, *39*, 807 – 814; q) B. V. R. Chowdari, G. V. S. Rao, S. Y. Chow, *Solid State Ionics* **2001**, *140*, 55 – 62.

[33] R. Stoyanova, E. Zhecheva, E. Kuzmanova, R. Alcantara, P. Lavela, J. L. Tirado, *Solid State Ionics* **2000**, *128*, 1 – 10.

[34] G. Ceder, M. K. Aydinol, A. F. Kohan, *Comput. Mater. Sci.* **1997**, *8*, 161 – 169.

[35] a) Y. I. Jang, B. Y. Huang, H. F. Wang, G. R. Maskaly, G. Ceder, D. R. Sadoway, Y. M. Chiang, H. Liu, H. Tamura, *J. Power Sources* **1999**, *81*, 589 – 593; b) G. X. Wang, S. Zhong, D. H. Bradhurst, S. X. Dou, H. K. Liu, *Solid State Ionics* **1999**, *116*, 271 – 277; c) S. H. Park, K. S. Park, Y. K. Sun, K. S. Nahm, Y. S. Lee, M. Yoshio, *Electrochim. Acta* **2001**, *46*, 1215 – 1222; d) M. Guilmard, A. Rougier, A. Grune, L. Croguennec, C. Delmas, *J. Power Sources* **2003**, *115*, 305 – 314; e) Z. Liu, H. Zhen, Y. Kim, C. Liang, *J. Power Sources* **2011**, *196*, 10201 – 10206.

[36] a) A. Yu, G. V. S. Rao, B. V. R. Chowdari, *Solid State Ionics* **2000**, *135*, 131 – 135; b) C. Pouillerie, L. Croguennec, C. Delmas, *Solid State Ionics* **2000**, *132*, 15 – 29; c) C. Pouillerie, L. Croguennec, P. Biensan, P. Willmann, C. Delmas, *J. Electrochem. Soc.* **2000**, *147*, 2061 – 2069; d) C. Julien, G. A. Nazri, A. Rougier, *Solid State Ionics* **2000**, *135*, 121 – 130; e) C. Chun-Chieh, K. Jin Yong, N. K. Prashant, *J. Electrochem. Soc.* **2000**, *147*, 1722 – 1729.

[37] a) L. Croguennec, E. Suard, P. Willmann, C. Delmas, *Chem. Mater.* **2002**, *14*, 2149 – 2157; b) J. Kim, K. Amine, *Electrochem. Commun.* **2001**, *3*, 52 – 55; c) K. C. Kam, M. M. Doeff, *J. Mater. Chem.* **2011**, *21*, 9991 – 9993; d) K. C. Kam, A. Mehta, J. T. Heron, M. M. Doeff, *J. Electrochem. Soc.* **2012**, *159*, A1383 – A1392.

[38] a) P. Mohan, K. A. Kumar, G. P. Kalaignan, V. S. Muralidharan, *J. Solid State Electrochem.* **2012**, *16*, 3695 – 3702; b) V. R. Galakhov, E. Z. Kurmaev, S. Uhlenbrock, M. Neumann, D. G. Kellerman, V. S. Gorshkov, *Solid State Commun.* **1995**, *95*, 347 – 351.

[39] Y. Nishida, Y. Nakane, T. Satoh, *J. Power Sources* **1997**, *68*, 561 – 564.

[40] a) M. Y. Song, I. H. Kwon, J. Song, S. Shim, *J. Appl. Electrochem.* **2009**, *39*, 617 – 625; b) M. Song, I. Kwon, *J. Alloys Compd.* **2009**, *484*, 591 – 596; c) D. G. Kellerman, E. V. Shalaeva, A. I. Gusev, *Phys. Solid State* **2004**, *46*, 1686 – 1692.

[41] C. Delmas, I. Saadoune, A. Rougier, *J. Power Sources* **1993**, *44*, 595 – 602.

[42] a) A. Hirano, R. Kanno, Y. Kawamoto, Y. Nitta, K. Okamura, T. Kamiyama, F. Izumi, *J. Solid State Chem.* **1997**, *134*, 1 – 4; b) T. Ohzuku, Y. Makimura, *Chem. Lett.* **2001**, 744 – 745.

[43] H.-J. Noh, S. Youn, C. S. Yoon, Y.-K. Sun, *J. Power Sources* **2013**, *233*, 121 – 130.

[44] W. M. Liu, G. R. Hu, Z. D. Peng, K. Du, Y. B. Cao, Q. Liu, *Chin. Chem. Lett.* **2011**, *22*, 1099 – 1102.

[45] a) T. J. Park, J. B. Lim, J. T. Son, *Bull. Korean Chem. Soc.* **2014**, *35*, 357 – 364; b) W. M. Liu, G. R. Hu, K. Du, Z. D. Peng, Y. B. Cao, *J. Power Sources* **2013**, *230*, 201 – 206; c) S.-M. Bak, K.-W. Nam, W. Chang, X. Yu, E. Hu, S. Hwang, E. A. Stach, K.-B. Kim, K. Y. Chung, X.-Q. Yang, *Chem. Mater.* **2013**, *25*, 337 – 351; d) Y. Makimura, S. J. Zheng, Y. Ikuhara, Y. Ukyo, *J. Electrochem. Soc.* **2012**, *159*, A1070 – A1073; e) S. Yoon, C. W. Lee, Y. S. Bae, I. Hwang, Y. K. Park, J. H. Song, *Electrochem. Solid-State Lett.* **2009**, *12*, A211 – A214.

[46] a) M. Guilmard, L. Croguennec, D. Denux, *Chem. Mater.* **2003**, *15*, 4476 – 4483; b) M. Guilmard, C. Pouillerie, L. Croguennec, C. Delmas, *Solid State Ionics* **2003**, *160*, 39 – 50.
[47] M. Broussely, P. Biensan, B. Simon, *Electrochim. Acta* **1999**, *45*, 3 – 22.
[48] a) C. Pouillerie, F. Perton, P. Biensan, J. P. Peres, M. Broussely, C. Delmas, *J. Power Sources* **2001**, *96*, 293 – 302; b) J. Cho, *Chem. Mater.* **2000**, *12*, 3089 – 3094; c) C. C. Chang, J. Y. Kim, P. N. Kumta, *J. Power Sources* **2000**, *89*, 56 – 63.
[49] a) M. J. Lee, S. Lee, P. Oh, Y. Kim, J. Cho, *Nano Lett.* **2014**, *14*, 993 – 999; b) Y. K. Sun, S. T. Myung, B. C. Park, J. Prakash, I. Belharouak, K. Amine, *Nat. Mater.* **2009**, *8*, 320 – 324.
[50] a) J. N. Reimers, E. Rossen, C. D. Jones, J. R. Dahn, *Solid State Ionics* **1993**, *61*, 335 – 344; b) G. Prado, A. Rougier, L. Fournes, C. Delmas, *J. Electrochem. Soc.* **2000**, *147*, 2880 – 2887; c) C. Delmas, M. Menetrier, L. Croguennec, S. Levasseur, J. P. Peres, C. Pouillerie, G. Prado, L. Fournes, F. Weill, *Int. J. Inorg. Mater.* **1999**, *1*, 11 – 19.
[51] a) L. J. Fu, H. Liu, C. Li, Y. P. Wu, E. Rahm, R. Holze, H. Q. Wu, *Solid State Sci.* **2006**, *8*, 113 – 128; b) C. Li, H. P. Zhang, L. J. Fu, H. Liu, Y. P. Wu, E. Ram, R. Holze, H. Q. Wu, *Electrochim. Acta* **2006**, *51*, 3872 – 3883; c) Z. H. Chen, Y. Qin, K. Amine, Y. K. Sun, *J. Mater. Chem.* **2010**, *20*, 7606 – 7612; d) K. T. Lee, S. Jeong, J. Cho, *Acc. Chem. Res.* **2013**, *46*, 1161 – 1170; e) Y. Oh, S. Nam, S. Wi, S. Hong, B. Park, *Electron. Mater. Lett.* **2012**, *8*, 91 – 105; f) A. Mauger, C. Julien, *Ionics* **2014**, *20*, 751 – 787.
[52] J. Cho, T. J. Kim, Y. J. Kim, B. Park, *Electrochem. Solid-State Lett.* **2001**, *4*, A159 – A161.
[53] a) J. Xiang, C. Chang, L. Yuan, J. Sun, *Electrochem. Commun.* **2008**, *10*, 1360 – 1363; b) S. T. Myung, K. Izumi, S. Komaba, H. Yashiro, H. J. Bang, Y. K. Sun, N. Kumagai, *J. Phys. Chem. C* **2007**, *111*, 4061 – 4067; c) S.-T. Myung, K. Izumi, S. Komaba, Y.-K. Sun, H. Yashiro, N. Kumagai, *Chem. Mater.* **2005**, *17*, 3695 – 3704.
[54] a) H.-J. Kweon, S. J. Kim, D. G. Park, *J. Power Sources* **2000**, *88*, 255 – 261; b) H.-J. Kweon, *Electrochem. Solid-State Lett.* **1999**, *3*, 128 – 130; c) W.-S. Yoon, K.-W. Nam, D. Jang, K. Y. Chung, J. Hanson, J.-M. Chen, X.-Q. Yang, *J. Power Sources* **2012**, *217*, 128 – 134.
[55] a) H. Omanda, T. Brousse, C. Marhic, D. M. Schleich, *J. Electrochem. Soc.* **2004**, *151*, A922 – A929; b) S. Sim, P. Oh, S. Park, J. Cho, *Adv. Mater.* **2013**, *25*, 4498 – 4503; c) Y. Cho, Y. S. Lee, S. A. Park, Y. Lee, J. Cho, *Electrochim. Acta* **2010**, *56*, 333 – 339.
[56] G. G. Amatucci, J.-M. Tarascon, Bell Communications Research, Inc., Morristown, NJ, **1998**.
[57] S. M. Lee, S. H. Oh, J. P. Ahn, W. I. Cho, H. Jang, *J. Power Sources* **2006**, *159*, 1334 – 1339.
[58] S. Yoon, K.-N. Jung, S.-H. Yeon, C. S. Jin, K.-H. Shin, *J. Electroanal. Chem.* **2012**, *683*, 88 – 93.
[59] J. Ying, C. Wan, C. Jiang, *J. Power Sources* **2001**, *102*, 162 – 166.
[60] a) Y. K. Sun, S. T. Myung, M. H. Kim, J. Prakash, K. Amine, *J. Am. Chem. Soc.* **2005**, *127*, 13411 – 13418; b) Y. K. Sun, S. T. Myung, H. S. Shin, Y. C. Bae, C. S. Yoon, *J. Phys. Chem. B* **2006**, *110*, 6810 – 6815; c) G. M. Koenig, I. Belharouak, H. Deng, Y.-K. Sun, K. Amine, *Chem. Mater.* **2011**, *23*, 1954 – 1963; d) Y.-K. Sun, S.-T. Myung, B.-C. Park, K. Amine, *Chem. Mater.* **2006**, *18*, 5159 – 5163.
[61] a) Y. K. Sun, Z. H. Chen, H. J. Noh, D. J. Lee, H. G. Jung, Y. Ren, S. Wang, C. S. Yoon, S. T. Myung, K. Amine, *Nat. Mater.* **2012**, *11*, 942 – 947; b) Y. K. Sun, D. H. Kim, C. S. Yoon, S. T. Myung, J. Prakash, K. Amine, *Adv. Funct. Mater.* **2010**, *20*, 485 – 491; c) See Ref. [49b].
[62] Y. Cho, S. Lee, Y. Lee, T. Hong, J. Cho, *Adv. Energy Mater.* **2011**, *1*, 821 – 828.
[63] a) A. T. Appapillai, A. N. Mansour, J. Cho, Y. Shao-Horn, *Chem. Mater.* **2007**, *19*, 5748 – 5757; b) Y.-C. Lu, A. N. Mansour, N. Yabuuchi, Y. Shao-Horn, *Chem. Mater.* **2009**, *21*, 4408 – 4424.
[64] J. Cho, T. J. Kim, J. Kim, M. Noh, B. Park, *J. Electrochem. Soc.* **2004**, *151*, A1899 – A1904.
[65] G.-R. Hu, X.-R. Deng, Z.-D. Peng, K. Du, *Electrochim. Acta* **2008**, *53*, 2567 – 2573.
[66] J. Cho, H. Kim, B. Park, *J. Electrochem. Soc.* **2004**, *151*, A1707 – A1711.
[67] Y. Zeng, J. He, *J. Power Sources* **2009**, *189*, 519 – 521.
[68] X. Ma, C. Wang, X. Han, J. Sun, *J. Alloys Compd.* **2008**, *453*, 352 – 355.
[69] Y. Kim, J. Cho, *J. Electrochem. Soc.* **2007**, *154*, A495 – A499.
[70] J. Eom, K. S. Ryu, J. Cho, *J. Electrochem. Soc.* **2008**, *155*, A228 – A233.
[71] K. S. Ryu, S. H. Lee, B. K. Koo, J. W. Lee, K. M. Kim, Y. J. Park, *J. Appl. Electrochem.* **2008**, *38*, 1385 – 1390.
[72] M. Vijayakumar, S. Selvasekarapandian, *Cryst. Res. Technol.* **2004**, *39*, 611 – 616.
[73] D.-J. Lee, B. Scrosati, Y.-K. Sun, *J. Power Sources* **2011**, *196*, 7742 – 7746.
[74] S. Hwang, W. Chang, S. M. Kim, D. Su, D. H. Kim, J. Y. Lee, K. Y. Chung, E. A. Stach, *Chem. Mater.* **2014**, *26*, 1084 – 1092.
[75] L. Wu, K.-W. Nam, X. Wang, Y. Zhou, J.-C. Zheng, X.-Q. Yang, Y. Zhu, *Chem. Mater.* **2011**, *23*, 3953 – 3960.
[76] Z. R. Zhang, J. Li, Y. Yang, *Electrochim. Acta* **2006**, *52*, 1442 – 1450.
[77] a) See Ref. [21]; b) S. J. Zheng, R. Huang, Y. Makimura, Y. Ukyo, C. A. J. Fisher, T. Hirayama, Y. Ikuhara, *J. Electrochem. Soc.* **2011**, *158*, A357 – A362.
[78] E. J. Lee, Z. Chen, H. J. Noh, S. C. Nam, S. Kang, D. H. Kim, K. Amine, Y. K. Sun, *Nano Lett.* **2014**, *14*, 4873 – 4880.
[79] a) H. Wang, *J. Electrochem. Soc.* **1999**, *146*, 473 – 480; b) H. Wang, Y.-I. Jang, B. Huang, D. R. Sadoway, Y.-M. Chiang, *J. Power Sources* **1999**, *81 – 82*, 594 – 598.
[80] Y. Shin, A. Manthiram, *Electrochem. Solid-State Lett.* **2002**, *5*, A55.
[81] D. J. Miller, C. Proff, J. G. Wen, D. P. Abraham, J. Bareno, *Adv. Energy Mater.* **2013**, *3*, 1098 – 1103.
[82] S. Watanabe, M. Kinoshita, T. Hosokawa, K. Morigaki, K. Nakura, *J. Power Sources* **2014**, *258*, 210 – 217.
[83] P. Oh, M. Ko, S. Myeong, Y. Kim, J. Cho, *Adv. Energy Mater.* **2014**, DOI: 10.1002/aenm.201470087.
[84] J. K. Ngala, N. A. Chernova, M. Ma, M. Mamak, P. Y. Zavalij, M. S. Whittingham, *J. Mater. Chem.* **2004**, *14*, 214 – 220.
[85] K. S. Lee, S. T. Myung, K. Amine, H. Yashiro, Y. K. Sun, *J. Electrochem. Soc.* **2007**, *154*, A971 – A977.
[86] See Ref. [36c].
[87] Y. K. Sun, B. R. Lee, H. J. Noh, H. M. Wu, S. T. Myung, K. Amine, *J. Mater. Chem.* **2011**, *21*, 10108 – 10112.
[88] M. H. Park, M. Noh, S. Lee, M. Ko, S. Chae, S. Sim, S. Choi, H. Kim, H. Nam, S. Park, J. Cho, *Nano Lett.* **2014**, *14*, 4083 – 4089.
[89] K.-W. Nam, S.-M. Bak, E. Hu, X. Yu, Y. Zhou, X. Wang, L. Wu, Y. Zhu, K.-Y. Chung, X.-Q. Yang, *Adv. Funct. Mater.* **2013**, *23*, 1047 – 1063.

Received: September 18, 2014
Published online: March 20, 2015